Am J Cancer Res 2025;15(7):3106-3127
www.ajcr.us /ISSN:2156-6976/ajcr0162545

Original Article

Multi-omics profiling reveals PLEKHA6 as a modulator of β-catenin signaling and therapeutic vulnerability in lung adenocarcinoma

Bing-Hua Su[1*], Sachin Kumar[2,3*], Li-Hsin Cheng[4], Wan-Jung Chang[5], Dahlak Daniel Solomon[2,6], Ching-Chung Ko[7,8,9], Chung-Chieh Chiao[3,10], Do Thi Minh Xuan[11], Juan Lorell Ngadio[2,12], Christophorus Manuel Heryanto[2,13], Bianca Tobias William[2,14], Fitria Sari Wulandari[2,15], Hao-Chien Yang[15], Hung-Yun Lin[2,16,17,18,19], Chih-Yang Wang[2,10,16], Ming-Cheng Tsai[20,21], Ming-Derg Lai[22,23]

[1]School of Respiratory Therapy, College of Medicine, Taipei Medical University, Taipei 11031, Taiwan; [2]Graduate Institute of Cancer Biology and Drug Discovery, College of Medical Science and Technology, Taipei Medical University, Taipei 11031, Taiwan; [3]Faculty of Applied Sciences and Biotechnology, Shoolini University of Biotechnology and Management Sciences, Himachal Pradesh 173229, India; [4]Core Laboratory of Organoids Technology, Office of R&D, Taipei Medical University, Taipei 11031, Taiwan; [5]Division of Pulmonology, Department of Internal Medicine, Wan Fang Hospital, Taipei Medical University, Taipei 11031, Taiwan; [6]Yogananda School of AI Computers and Data Sciences, Shoolini University, Solan 173229, India; [7]Department of Medical Imaging, Chi-Mei Medical Center, Tainan 71004, Taiwan; [8]Department of Health and Nutrition, Chia Nan University of Pharmacy and Science, Tainan 71710, Taiwan; [9]School of Medicine, College of Medicine, National Sun Yat-Sen University, Kaohsiung 80424, Taiwan; [10]PhD Program for Cancer Molecular Biology and Drug Discovery, College of Medical Science and Technology, Taipei Medical University, Taipei 11031, Taiwan; [11]Faculty of Pharmacy, Van Lang University, 69/68 Dang Thuy Tram Street, Ward 13, Binh Thanh District, Ho Chi Minh 70000, Vietnam; [12]Department of Bioinformatics, School of Life Sciences, Indonesia International Institute for Life Sciences, Jl Pulomas Barat Kav 88, Jakarta Timur 13210, Indonesia; [13]Department of Biotechnology, Faculty of Applied Sciences, UCSI University, No. 1, Jalan UCSI, UCSI Heights, Cheras 56000, Kuala Lumpur, Malaysia; [14]Department of Biomedicine, School of Life Sciences, Indonesia International Institute for Life Sciences, Jl Pulomas Barat Kav 88, Jakarta Timur 13210, Indonesia; [15]Department of Surgery, Division of Neurosurgery, Shuang Ho Hospital, Taipei Medical University, New Taipei City 23561, Taiwan; [16]TMU Research Center of Cancer Translational Medicine, Taipei Medical University, Taipei 11031, Taiwan; [17]Cancer Center, Wan Fang Hospital, Taipei Medical University, Taipei 11031, Taiwan; [18]Traditional Herbal Medicine Research Center of Taipei Medical University Hospital, Taipei Medical University, Taipei 11031, Taiwan; [19]Pharmaceutical Research Institute, Albany College of Pharmacy and Health Sciences, Rensselaer, NY 12144, USA; [20]School of Medicine, Fu Jen Catholic University, New Taipei City 242, Taiwan; [21]Department of Neurosurgery, Shin-Kong Wu Ho-Su Memorial Hospital, 95 Wen-Chang Road, Shih-Lin District, Taipei 111045, Taiwan; [22]Department of Biochemistry and Molecular Biology, National Cheng Kung University, Tainan 70101, Taiwan; [23]Institute of Basic Medical Sciences, College of Medicine, National Cheng Kung University, Tainan 70101, Taiwan. [*]Equal contributors.

Received December 9, 2024; Accepted June 25, 2025; Epub July 15, 2025; Published July 30, 2025

Abstract: Lung adenocarcinoma (LUAD) remains the most prevalent and lethal subtype of lung cancer, largely due to late diagnosis and therapeutic resistance. In this study, we conducted a comprehensive multi-omics analysis to characterize the pleckstrin homology domain-containing (PLEKHA) family gene in LUAD. Among the eight members, PLEKHA6 was uniquely overexpressed in LUAD tissues and significantly associated with poor prognosis. Integrated bulk RNA-Seq, single-cell RNA-Seq, DNA methylation, and pharmacogenomic analyses identified PLEKHA6 as a key modulator of oncogenic processes, including Wnt/β-catenin signaling, cadherin-mediated adhesion, and cytoskeletal remodeling. Functional assays in A549 LUAD cells revealed that PLEKHA6 knockdown suppressed β-catenin and VE-cadherin expression, leading to impaired proliferation, migration, and colony formation, along with enhanced apoptosis and cell cycle arrest. Single-cell RNA sequencing demonstrated a correlation between PLEKHA6 expression and tumor-associated macrophage (TAM) infiltration, implicating PLEKHA6 in immune remodeling within the tumor microenvironment (TME). Drug sensitivity analysis and molecular docking further identified potential therapeutic drugs targeting PLEKHA6-expressing LUAD cells. Collectively, our findings establish PLEKHA6 as a novel

https://doi.org/10.62347/NVVF8441

oncogenic driver and immune modulator in LUAD, supporting its potential as both a prognostic biomarker and a therapeutic target for precision oncology.

Keywords: Pleckstrin homology domain-containing family A6 (PLEKHA6), lung adenocarcinoma, β-catenin, tumor microenvironment, single-cell RNA-seq, drug discovery

Introduction

Lung adenocarcinoma (LUAD) is the most common subtype of non-small cell lung cancer (NSCLC), accounting for approximately 40% of all lung cancer cases [1, 2]. Despite advances in diagnostic techniques and therapeutic strategies, the prognosis for patients with LUAD remains poor, with a five-year survival rate of less than 20% globally. The high mortality rate is often attributed to late-stage diagnosis and the heterogeneous nature of the disease, which complicates treatment approaches [3-7]. Consequently, there is an urgent need for reliable biomarkers that can predict patient prognosis, and potentially serve as therapeutic targets [8-10].

Recent advances in high-throughput sequencing and bioinformatics have facilitated the identification of novel biomarkers that may play crucial roles in cancer progression and patient outcomes. Among these, the pleckstrin homology domain-containing family A (PLEKHA) member genes have garnered attention due to their involvement in various cellular processes, including signal transduction, cytoskeletal dynamics, and membrane trafficking. The PLEKHA family consists of eight members: PLEKHA1, PLEKHA2, PLEKHA3, PLEKHA4, PLEKHA5, PLEKHA6, PLEKHA7, and PLEKHA8. As the name suggests, the PLEKHA family codes for proteins that contain pleckstrin homology (PH) domain which is known to bind phosphatidylinositol lipids, such as the PIP_3 and PIP_2, as well as other proteins to the plasma membrane [11]. Thus, the PLEKHA family has essential roles in a variety of intracellular downstream signaling pathways. These genes have been implicated in a variety of cancers; however, their specific roles and clinical relevance in LUAD remain underexplored [12, 13]. For instance, Jeung et al. suggested that knockdown of PLEKHA7 could inhibit the growth of colorectal cancer which harbors mutant-KRAS [14]. Moreover, PLEKHA5 is a downstream effector of Met signaling in diffuse-type gastric carcinoma (DGC) with met gene amplification, suggesting that targeting PLEKHA5 could be a potential strategy to combat Met inhibitor resistance [15].

In this study, we performed an integrative multi-omics analysis to investigate the expression patterns, functional roles, and clinical significance of the PLEKHA gene family in LUAD. Among the eight family members, PLEKHA6 emerged as the most significantly overexpressed gene in LUAD tissues and was uniquely associated with poor overall survival, distinguishing it from other PLEKHA genes with no significant prognostic value. We further examined its relationship with immune cell infiltration, β-catenin activation, and drug sensitivity (**Figure 1**). Our findings reveal that PLEKHA6 acts as a clinically relevant immune-modulatory oncogene that promotes LUAD progression, offering novel insights into therapeutic vulnerabilities and potential biomarker.

Material and methods

Gene expression and prognostic analysis

This study employs a comprehensive bioinformatics approach to investigate the prognostic significance of the PLEKHA gene family, with a specific focus on PLEKHA6 in LUAD. Publicly available datasets were utilized for the analysis, including gene expression data from The Cancer Genome Atlas (TCGA) and the Gene Expression Omnibus (GEO). Additionally, expression data from normal lung tissues were obtained from the Genotype-Tissue Expression (GTEx) project to serve as a comparative baseline [16]. To gain insights into the functional implications of PLEKHA6-regulated genes, we employed the clusterProfiler R package [17], Omics Playground v.3.4.1 [18], and SRplot platform [19] for conducting functional enrichment analyses [20-22]. To evaluate the prognostic value of PLEKHA6 in LUAD, Kaplan-Meier survival analyses were performed using GEPIA and UALCAN, based on their predefined cut-off criteria [23-25]. Patients were stratified into high- and low-expression groups according to the median expression level of PLEKHA6 as previous described [26-28].

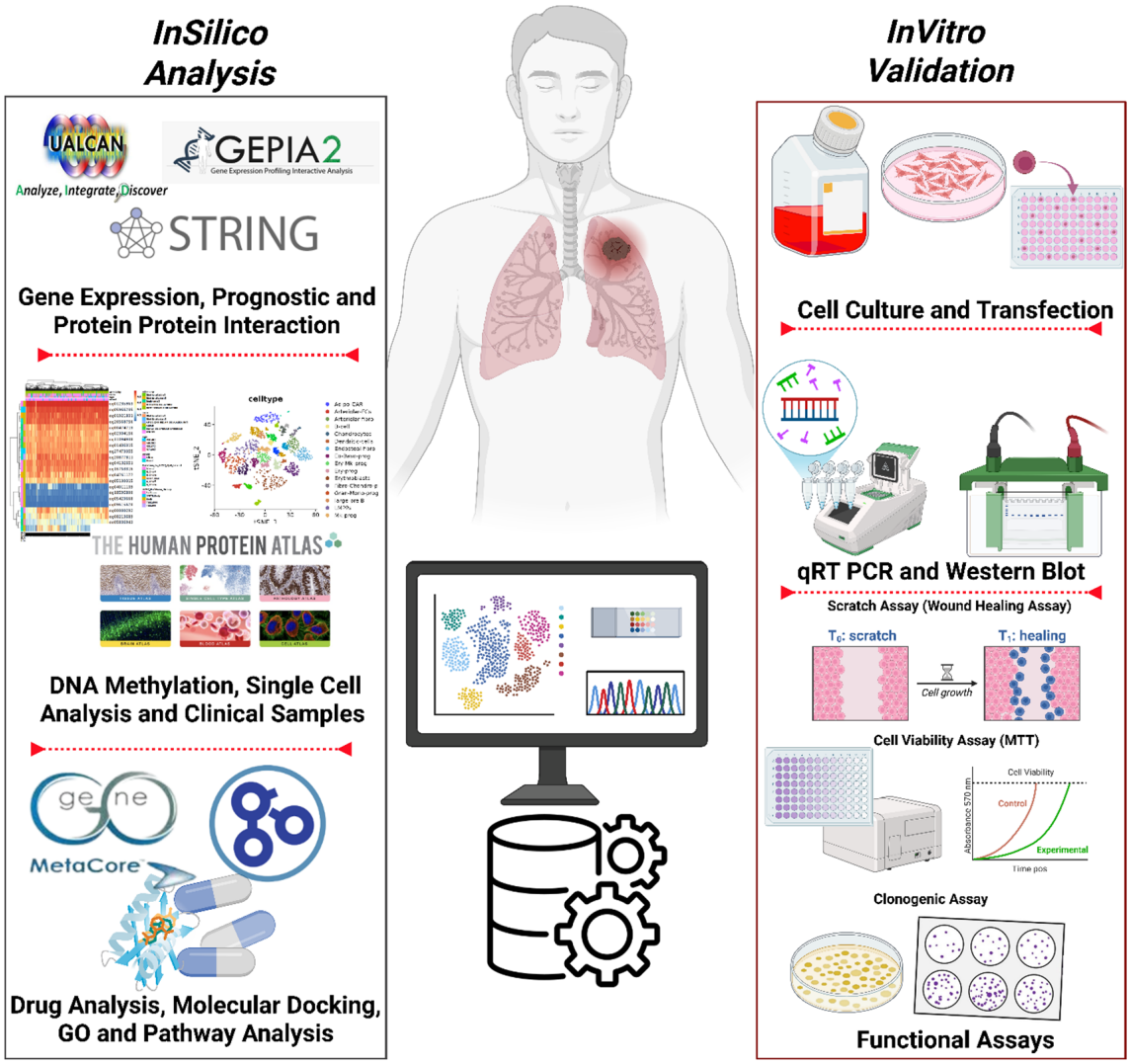

Figure 1. Schematic overview of the study workflow integrating multi-omics analysis, survival prediction, immune profiling, drug sensitivity screening, and molecular docking to investigate the role of PLEKHA6 in LUAD.

DNA methylation analysis and cancer cell line encyclopedia (CCLE)

The MethSurv database (https://biit.cs.ut.ee/methsurv/) was utilized to analyze single CpG methylation patterns and generate heatmaps of distinct DNA methylated regions. The DNA methylation values were represented as beta values, which range from 0 to 1. The methylation level at each CpG site was calculated using the formula M/(M + U + 100), where 'M' represents the intensity values of methylated DNA and 'U' represents the intensity values of unmethylated DNA. This analysis provided insights into the epigenetic regulation of PLEKHA6 and its potential role in LUAD progression [29-31]. For the CCLE dataset through the cBioPortal platform (https://www.cbioportal.org/), which integrates diverse genomic data types, including somatic mutations, copy-number alterations, and mRNA expression profiles. The CCLE database includes extensive characterizations of over 1,000 cancer cell lines derived from various tumor types. We queried the expression levels of PLEKHA6 and examined its genetic alterations across different LUAD cell lines [32].

Integrated pathway enrichment, drug sensitivity prediction, and molecular docking analysis of PLEKHA6 in LUAD

MetaCore pathway analysis was employed to delve into the specific signaling networks and

biological processes linked to PLEKHA6. The platform explored the interactions between PLEKHA6 and other key regulatory proteins, shedding light on its potential role as a therapeutic target [33-36]. To identify pharmacological compounds potentially targeting PLEKHA6, drug sensitivity analysis was conducted using the Genomics of Drug Sensitivity in Cancer Analysis (GSCA) platform (https://guolab.wchscu.cn/GSCA/#/drug) [37]. GSCA integrates transcriptomic and pharmacogenomic data to associate gene expression with drug response profiles. Compounds were ranked based on their correlation with PLEKHA6 expression across multiple cancer datasets, highlighting several agents for further validation. To further validate the interaction of candidate drugs with PLEKHA6, molecular docking analysis was performed. Selected compounds identified through GSCA and CTRP analyses, including Austocystin D, BX-912, Camptothecin, Doxorubicin, Etoposide, and Foretinib were subjected to docking simulations. Their 3D structures were retrieved from PubChem in SDF format and preprocessed using PyMol and AutoDockTools. The predicted structure of PLEKHA6 was obtained from AlphaFold3 (UniProt ID: Q9Y2H5), excluding low-confidence regions to ensure modeling accuracy. Binding site prediction was performed using the CastP-Fold server, and Pocket 6 was selected for docking based on its concordance with AlphaFold's predicted pathogenicity regions. AutoDock Vina was used to conduct docking simulations, with energy range and exhaustiveness set to 4 and 8, respectively. Ligand-protein interactions were visualized in 3D using PyMol and in 2D using LigPlot+ and Biovia Discovery Studio [38-41]. This integrated approach combining pathway enrichment, transcriptomic drug prediction, and molecular docking provides a comprehensive framework for identifying and validating small-molecule therapeutics targeting PLEKHA6 in LUAD.

Protein-protein interaction and single-cell RNA sequencing data acquisition and processing

The Search Tool for the Retrieval of Interacting Genes/Proteins (STRING) is an online resource designed to evaluate protein-protein interaction (PPI) networks. In this study, STRING version 10.5 was employed to assess potential PPI relationships among differentially expressed genes (DEGs) [42], and visualized using Cytoscape software version 3.6.0 [43-46]. The single-cell RNA sequencing (scRNA-seq) dataset used in this study was obtained from the previously published work by Travaglini et al. which offers a comprehensive cellular atlas of the human lung [47]. For the purposes of our analysis, only lung tissue samples were extracted from the processed dataset to investigate the TME in greater detail. The original dataset, available in Hierarchical Data Format version 5 (.h5ad), was converted to R Data Serialization (.rds) format using the convert Format function from the sceasy package (v0.0.7), ensuring compatibility with R-based analytical tools. The converted .rds file was then imported into the Seurat package (v5.1.0) for downstream processing and analysis [48, 49]. Comprehensive scRNA-seq analysis was performed using the SCP: Single Cell Pipeline (v0.5.6) which provides an integrated workflow for preprocessing, clustering, dimensionality reduction, and visualization. The final dataset consisted of 58,870 genes profiled across 35,685 individual cells, offering high-resolution insights into the cellular composition of lung tissue. Data visualization and heatmap generation were conducted using the Complex Heatmap package (v2.22.0) allowing for the identification of significant expression patterns and intercellular relationships within the TME [50].

Cell culture, RNA extraction, RT-qPCR, and western blot analysis

A549 human LUAD cells kindly provided from Prof. Chiou-Feng Lin (Taipei Medical University), the cells were cultured in DMEM (Corning, Cat. No. 90-113-PB) with 10% FBS (Avantor, Singapore) and 1% penicillin-streptomycin at 37°C with 5% CO_2 [51, 52]. Stable knockdown of PLEKHA6 was achieved using shRNA constructs from the National RNAi Core Facility (Academia Sinica, Taipei), with pLKO.1-shLacZ as control. Total RNA was extracted using the GENEzol™ TriRNA Pure Kit (Geneaid, Taiwan) and reverse-transcribed with PrimeScript RT Reagent Kit (Takara). RT-qPCR was conducted on a Roche LightCycler® 96 with TB Green® SYBR Green Master Mix (Takara). Primers for PLEKHA6, β-catenin, and VE-cadherin were from OriGene, normalized to GAPDH using the

2^-ΔΔCt method. Triplicate experiments were averaged and expressed as mean ± SD.

For Western blotting, proteins were extracted in RIPA buffer (Cyrusbio, Taiwan) with protease/phosphatase inhibitors, quantified using BCA assay (Omics Bio), and resolved by 10% SDS-PAGE. After PVDF membrane transfer and 5% BSA blocking, blots were probed overnight with primary antibodies: anti-PLEKHA6 (AbClonal A24210), anti-β-catenin (Cell Signaling Technology S33/37/T41), anti-VE-cadherin (AbClonal A0734), and anti-α-tubulin (Elabsciences E-AB-20036). Goat anti-mouse (AP124P) and goat anti-rabbit (AP132) HRP-conjugated antibodies (Sigma-Aldrich) were used as secondaries. Signal was visualized with ECL reagent (Thermo Scientific) using the e-BLOT Touch Imager.

Cell proliferation, colony formation, and wound-healing assays

Cell viability was evaluated by MTT assay. A549 cells (5×10^3/well) were seeded in 96-well plates and treated for 0, 24, 48, and 72 h. MTT reagent (0.5 mg/mL) was added for 4 h, and formazan crystals were solubilized in DMSO for absorbance reading at 570 nm. Colony formation assays involved seeding 1×10^3 cells/well in 6-well plates, culturing for 7 days, followed by ethanol fixation and methylene blue staining; colony size and number were quantified microscopically. For wound-healing assays, confluent monolayers were scratched using a 10-μL pipette tip and washed with PBS. Wound closure was monitored at 0 and 24 h using an Olympus IX73 microscope.

Statistical analysis

All statistical analyses were performed using R software (version 4.0.3). Data visualization, including heatmaps, boxplots, and survival curves, was carried out using ggplot2 and pheatmap packages [53-55]. The significance level for all statistical tests was set at $P < 0.05$. Data visualization and statistical analysis were conducted using ggplot2, SPSS (IBM, Armonk, NY, USA), and ImageJ (NIH, Bethesda, MD, USA). Results are expressed as mean ± standard deviation (SD) from at least three independent experiments. Statistical significance was assessed using one-way and two-way ANOVA.

Results

Differential expression of PLEKHA gene family in LUAD

Our comprehensive bioinformatics analysis revealed distinct expression patterns of the PLEKHA gene family across Pan-cancer and normal tissues (**Figure 2A**). Among them, PLEKHA3, PLEKHA5, PLEKHA6 PLEKHA7, and PLEKHA8 were significantly overexpressed in LUAD patients (p-value < 0.05). While PLEKHA1, PLEKHA2, and PLEKHA4 showed relatively low expression levels (**Figure 2A**). Boxplots demonstrated notably elevated PLEKHA6 expression in LUAD tissues compared to normal lung tissues, with a clear distinction between cancerous and non-cancerous samples and a positive correlation with tumor stage (**Figure 2B**). To validate these findings, we conducted an independent analysis using the GSE86958 dataset, which contains paired RNA expression profiles from six patients with invasive mucinous LUAD and adjacent normal lung tissues. The volcano plot generated via Limma differential expression analysis ($\log_2FC \pm 2$, $P < 0.05$) further highlighted PLEKHA family members (Supplementary Figure 1A), especially PLEKHA6, as significantly dysregulated. The distribution of significant gene alterations was visualized using a Manhattan plot, reinforcing the association of PLEKHA6 with LUAD tumorigenesis (Supplementary Figure 1B). A boxplot comparison confirmed significantly higher PLEKHA6 expression in tumors ($P = 0.0031$, Tukey's t-test; Supplementary Figure 1C). Analysis of PLEKHA6 expression in LUAD cell lines from the Cancer Cell Line Encyclopedia (CCLE) dataset revealed notably high levels in HCC78 and NCIH2106, both known for their aggressive tumor behavior [56], suggesting a potential link between PLEKHA6 expression and tumor aggressiveness (Supplementary Figure 2).

Across TCGA-LUAD samples, PLEKHA6 expression remained strongly elevated, particularly in advanced-stage tumors (**Figure 3A**). Correlation with clinicopathological features, including TP53 mutation, smoking history, age, gender, nodal status, and histology,was explored (Supplementary Figure 3A-F; Supplementary Tables 1, 2, 3, 4, 5, 6). Notably, TP53-mutant cases exhibited higher PLEKHA6 levels, align-

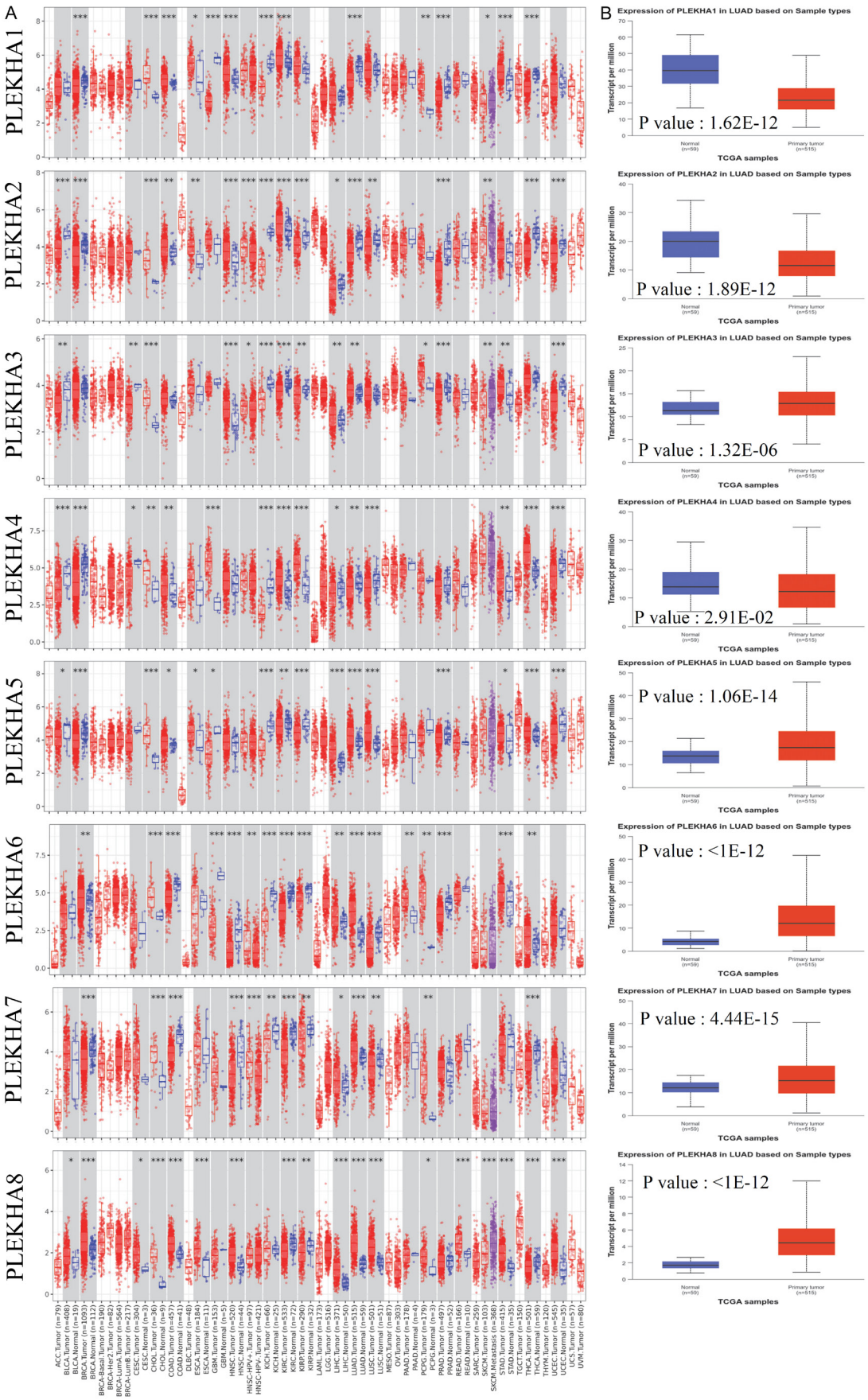
A
PLEKHA1
PLEKHA2
PLEKHA3
PLEKHA4
PLEKHA5
PLEKHA6
PLEKHA7
PLEKHA8
B
Expression of PLEKHA1 in LUAD based on Sample types
P value : 1.62E-12
Expression of PLEKHA2 in LUAD based on Sample types
P value : 1.89E-12
Expression of PLEKHA3 in LUAD based on Sample types
P value : 1.32E-06
Expression of PLEKHA4 in LUAD based on Sample types
P value : 2.91E-02
Expression of PLEKHA5 in LUAD based on Sample types
P value : 1.06E-14
Expression of PLEKHA6 in LUAD based on Sample types
P value : <1E-12
Expression of PLEKHA7 in LUAD based on Sample types
P value : 4.44E-15
Expression of PLEKHA8 in LUAD based on Sample types
P value : <1E-12
Transcript per million
Normal (n=59)
Primary tumor (n=515)
TCGA samples

Figure 2. Pan-cancer analysis of PLEKHA family genes from TCGA patients. A. Transcript levels of PLEKHA family genes in normal and cancer tissues from TCGA patients. B. Box plots indicate PLEKHA family mRNA expression in TCGA dataset, and PLEKHA6 had high expression levels in LUAD patients ($P < 0.05$ was considered significant).

ing with the role of TP53 in LUAD heterogeneity and progression [57, 58]. Associations with nodal metastasis and histological subtype further support its potential as a prognostic biomarker [59].

Survival analysis, DNA methylation and human protein atlas analysis of PLEKHA6 in LUAD

Kaplan-Meier and Cox regression analyses revealed that high PLEKHA6 expression significantly correlated with worse overall survival (**Figure 3B**) and reduced disease-free survival in LUAD patients, while other PLEKHA genes showed no prognostic significance [56]. These results were consistent across datasets and support PLEKHA6 as a robust prognostic biomarker (Supplementary Figure 4). DNA methylation analysis using MethSurv identified 36 CpG sites linked to PLEKHA6 expression (**Figure 4A**), with cg01720945 and cg26522351 significantly associated with patient survival (**Figure 4B**). Additionally, immunohistochemistry data from the Human Protein Atlas confirmed detectable PLEKHA6 protein expression in LUAD tissues. Of 12 cases analyzed, 2 showed moderate staining, 1 weak, and 9 negative using antibody HPA028152, this protein-level validation provides further evidence of the clinical relevance of PLEKHA6 in LUAD (Supplementary Figure 5).

Pathway enrichment and network analysis

Further network analysis using GO and STRING, as well as Cytoscape, identified key interactors of PLEKHA6, including proteins involved in cell adhesion and cytoskeletal remodeling, which are known to facilitate cancer cell dissemination (**Figure 5**). These findings are visualized in the protein-protein interaction (PPI) network presented in the STRING database, where PLEKHA6 is centrally positioned, interacting with multiple nodes implicated in cancer-related pathways (**Figure 6**). To elucidate the biological functions of PLEKHA6 in LUAD, pathway enrichment analysis was conducted using MetaCore. The analysis revealed that PLEKHA6 is significantly involved in several oncogenic pathways, including "Signal transduction_Ephrin-B signaling", "Cell adhesion_Classical cadherin-mediated cell adhesion", "Cell adhesion_Tight junctions", "PXR-mediated direct regulation of xenobiotic metabolizing enzymes/Rodent version", "Cytoskeleton remodeling_Regulation of actin cytoskeleton organization by the kinase effectors of Rho GTPases", "PXR-mediated direct regulation of xenobiotic metabolizing enzymes/Human version", "Androstenedione and testosterone biosynthesis and metabolism p.2", "G-protein signaling_RhoA activation", "Protein folding and maturation_Angiotensin system maturation", "Inhibition of Ephrin receptors in colorectal cancer", "G-protein signaling_Rac1 activation". These pathways are crucial for cell migration, invasion, and metastasis, which are key processes in cancer progression. The enriched pathways associated with PLEKHA6 highlight its role in regulating cellular processes critical to tumorigenesis. Notably, PLEKHA6 was also linked to the PXR-mediated regulation of xenobiotic metabolizing enzymes, suggesting a potential role in chemoresistance, which could contribute to the poor outcomes observed in patients with high PLEKHA6 expression (**Figure 7**; Supplementary Table 7). The involvement of PLEKHA6 in pathways related to cell adhesion, cytoskeletal dynamics, and drug metabolism suggests that targeting this gene or its downstream effectors could provide therapeutic benefits for LUAD patients, particularly those who do not respond to conventional therapies. The identification of these pathways also opens up the possibility of developing combination therapies that target multiple nodes in the signaling networks influenced by PLEKHA6, thereby enhancing treatment efficacy.

Single-cell analysis of PLEKHA6 in LUAD

To investigate the cellular localization and potential immunological role of PLEKHA6 in LUAD, we performed a detailed single-cell RNA sequencing (scRNA-seq) analysis using LUAD tumor datasets. The dot plot analysis (**Figure 8A**) demonstrated that PLEKHA6 expression was predominantly enriched in macrophage populations, as reflected by both the size and intensity of the dots, indicating a high propor-

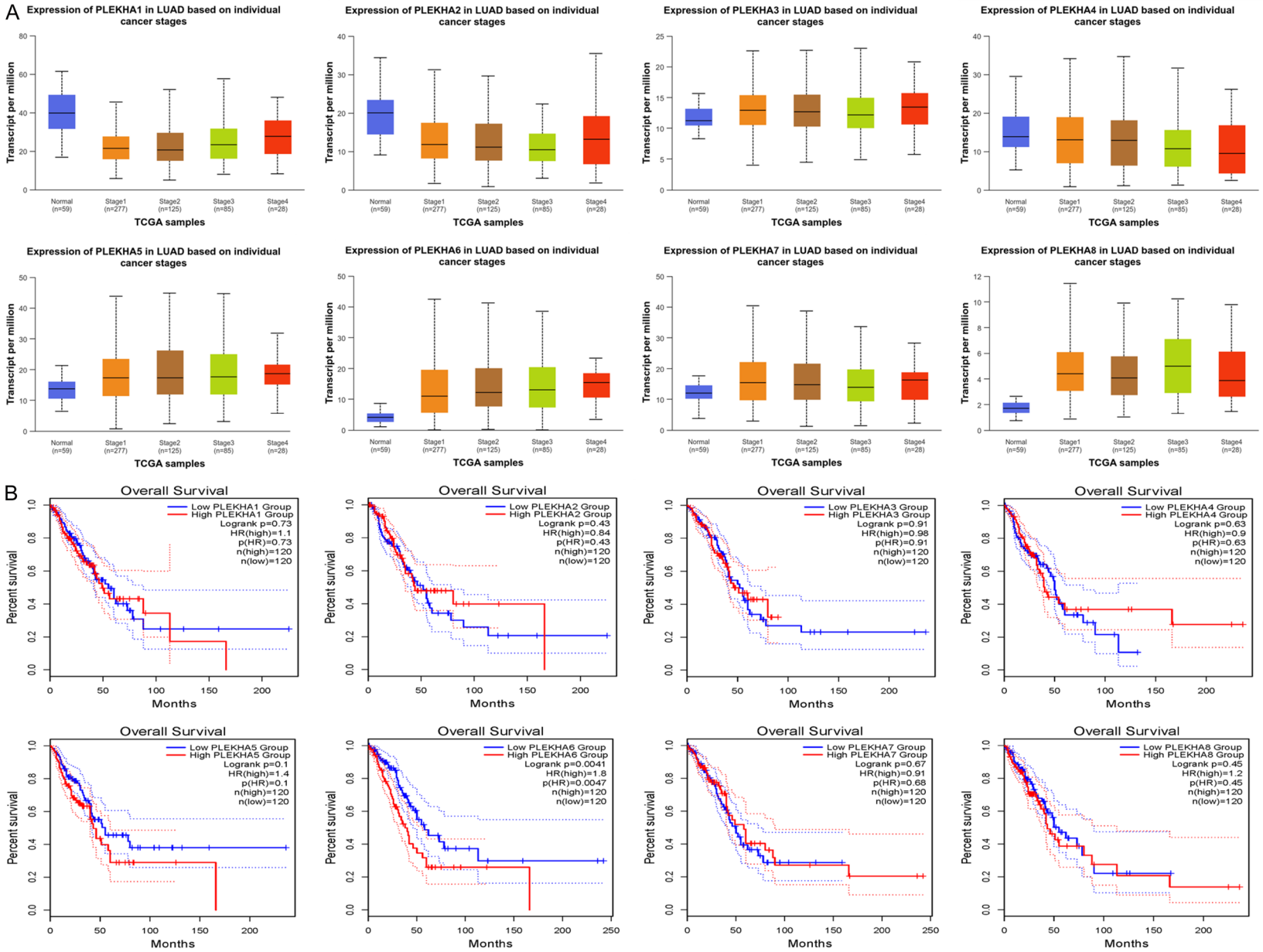
A
Expression of PLEKHA1 in LUAD based on individual cancer stages
Expression of PLEKHA2 in LUAD based on individual cancer stages
Expression of PLEKHA3 in LUAD based on individual cancer stages
Expression of PLEKHA4 in LUAD based on individual cancer stages
Expression of PLEKHA5 in LUAD based on individual cancer stages
Expression of PLEKHA6 in LUAD based on individual cancer stages
Expression of PLEKHA7 in LUAD based on individual cancer stages
Expression of PLEKHA8 in LUAD based on individual cancer stages
Transcript per million
Normal (n=59)
Stage1 (n=277)
Stage2 (n=125)
Stage3 (n=85)
Stage4 (n=28)
TCGA samples
B
Overall Survival
Low PLEKHA1 Group
High PLEKHA1 Group
Logrank p=0.73
HR(high)=1.1
p(HR)=0.73
n(high)=120
n(low)=120
Low PLEKHA2 Group
High PLEKHA2 Group
Logrank p=0.43
HR(high)=0.84
p(HR)=0.43
n(high)=120
n(low)=120
Low PLEKHA3 Group
High PLEKHA3 Group
Logrank p=0.91
HR(high)=0.98
p(HR)=0.91
n(high)=120
n(low)=120
Low PLEKHA4 Group
High PLEKHA4 Group
Logrank p=0.63
HR(high)=0.9
p(HR)=0.63
n(high)=120
n(low)=120
Low PLEKHA5 Group
High PLEKHA5 Group
Logrank p=0.1
HR(high)=1.4
p(HR)=0.1
n(high)=120
n(low)=120
Low PLEKHA6 Group
High PLEKHA6 Group
Logrank p=0.0041
HR(high)=1.8
p(HR)=0.0047
n(high)=120
n(low)=120
Low PLEKHA7 Group
High PLEKHA7 Group
Logrank p=0.67
HR(high)=0.91
p(HR)=0.68
n(high)=120
n(low)=120
Low PLEKHA8 Group
High PLEKHA8 Group
Logrank p=0.45
HR(high)=1.2
p(HR)=0.45
n(high)=120
n(low)=120
Percent survival
Months

Figure 3. Tumor stage and prognosis analysis of PLEKHA family genes from LUAD patients. A. A patient's tumor stage determined PLEKHA family genes expression levels in LUAD patients via the UALCAN platform ($P < 0.05$). B. Kaplan-Meier plot of PLEKHA family genes in LUAD patients for an overall survival analysis from TCGA patients via the GEPIA platform.

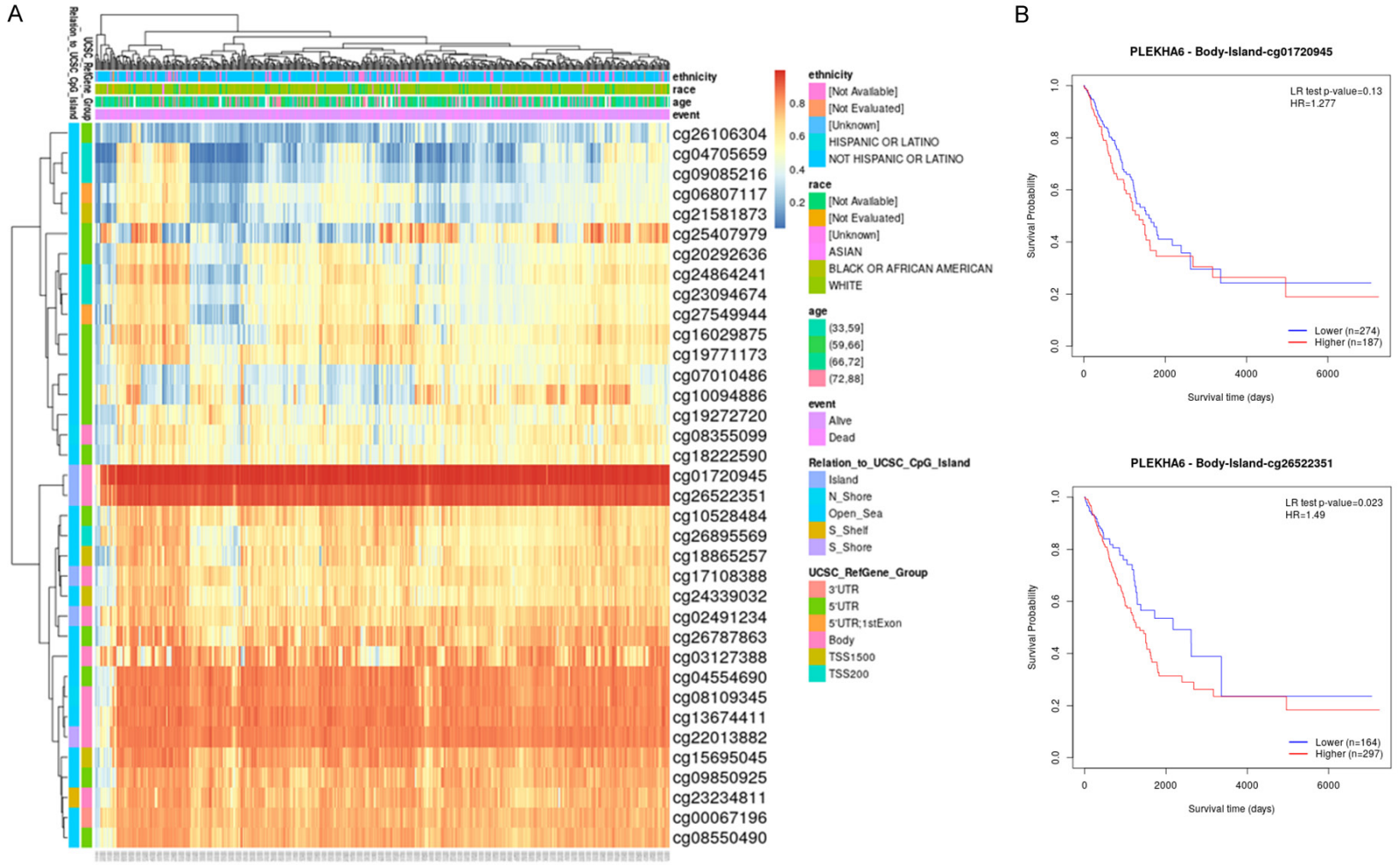

Figure 4. DNA methylation of PLEKHA6, and protein expression levels of PLEKHA6 in different LUAD. A. Heatmap of DNA methylation expression levels of PLEKHA6 in TCGA LUAD patients. B. The KM curves of PLEKHA6 related survival analysis with the methylation sites cg01720945 and cg26522351.

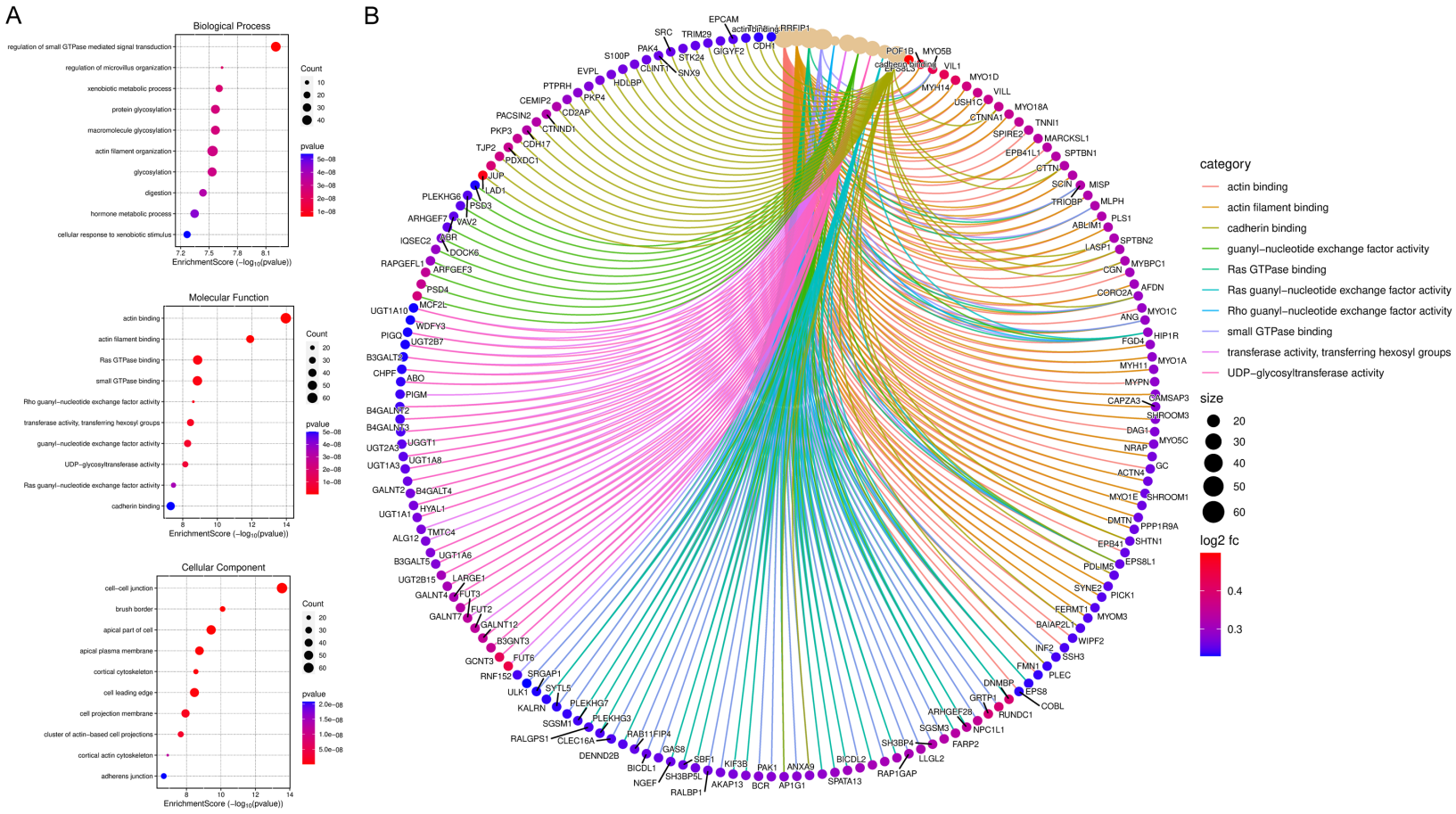

Figure 5. Functional and pathway enrichment analyses were performed specifically on genes co-expressed with PLEKHA6 in LUAD TCGA patients. A. The analysis involved gene ontology (GO) terms, including biological processes, cellular components, and molecular functions. Circle sizes in the visual representation of the results indicate the number of genes associated with each function, while colors of the bubbles correspond to *p* values, providing information about the statistical significance of the enrichment. B. Pathway analysis of PLEKHA6 co-expressed genes in the KEGG database.

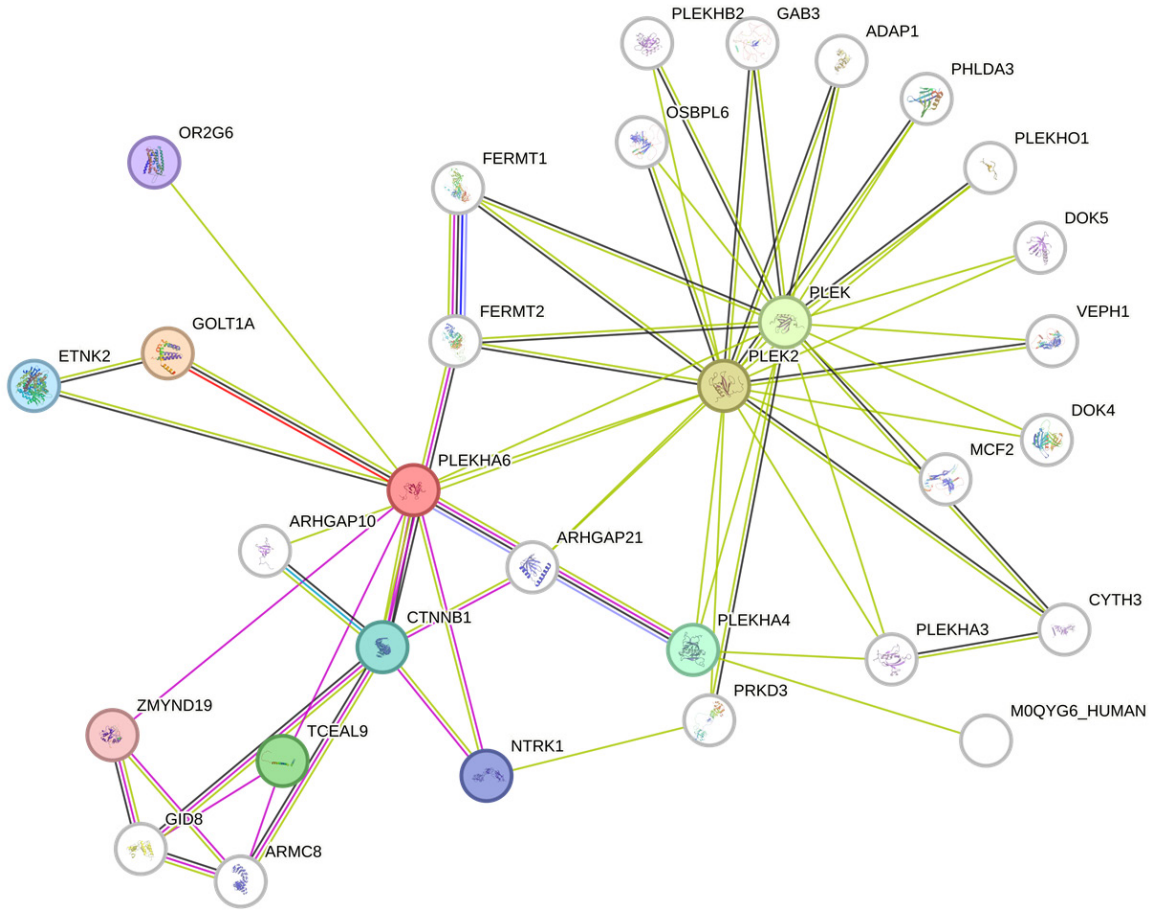

Figure 6. Protein-Protein Interactions (PPIs) of PLEKHA6 in STRING Database. Various types of evidence support the predicted interactions and are represented by different colored lines: red lines indicate the presence of fusion evidence, green lines denote neighborhood evidence, blue lines represent co-occurrence evidence, purple lines show experimental evidence, yellow lines indicate text mining evidence, light blue lines correspond to database evidence, and black lines represent co-expression evidence.

tion of PLEKHA6-positive macrophages and elevated transcript abundance. This macrophage-specific enrichment was further supported by a heatmap visualizing PLEKHA6 expression across annotated cell ontology classes (**Figure 8B**), which revealed consistently higher expression levels in macrophages relative to other immune, stromal, and epithelial populations.

To further delineate the spatial organization of PLEKHA6-expressing cells within the TME, we applied Uniform Manifold Approximation and Projection (UMAP) clustering. This analysis revealed distinct aggregation patterns of immune and stromal cell types (**Figure 8C**), with PLEKHA6-positive cells localizing predominantly within immune cell-rich clusters. A corresponding feature plot (**Figure 8D**) confirmed that regions of high PLEKHA6 expression spatially overlapped with clusters enriched for macrophages. This observation was validated by macrophage-specific UMAP annotation (**Figure 8E**), which showed a clear co-localization between PLEKHA6-expressing zones and tumor-associated macrophages (TAMs). TAMs are key mediators of tumor progression in LUAD, capable of regulating immune evasion, angiogenesis, and metabolic adaptation through diverse signaling pathways such as G-protein signaling, Ephrin-B signaling, and Rho GTPase-driven cytoskeletal remodeling. They exhibit functional plasticity and can polarize into M1-like (pro-inflammatory) or M2-like (pro-tumorigenic) phenotypes depending on the cues within the TME [52, 60, 61]. The selective upregulation of PLEKHA6 in TAMs suggests a role in reinforcing M2-like polarization, which is

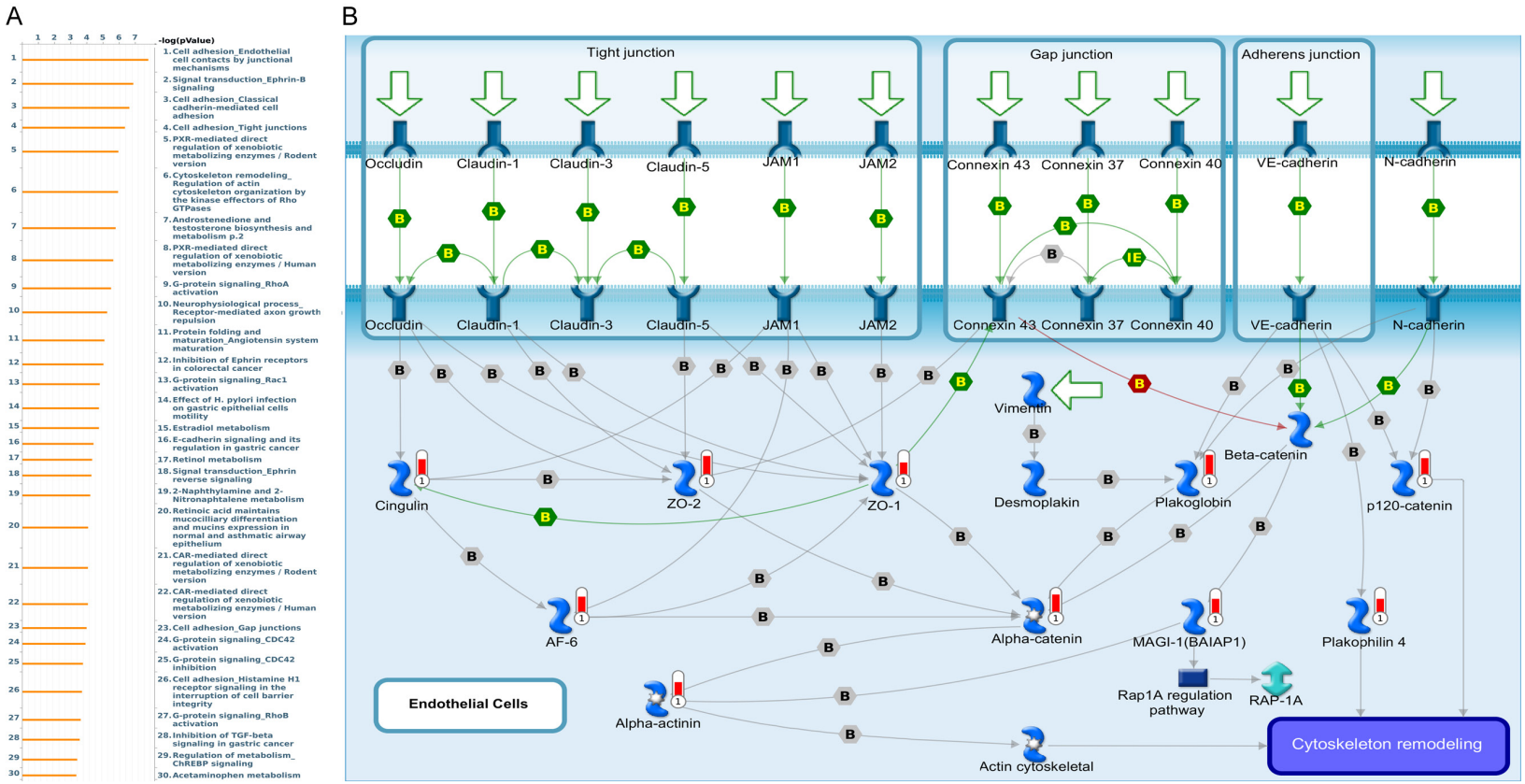

Figure 7. MetaCore pathway analysis of PLEKHA6 co-expressed genes in LUAD patients from TCGA. A. The MetaCore pathway enrichment analysis was conducted for genes co-expressed with PLEKHA6 in LUAD patients, revealing potential pathways involving these genes ranked by their log *p* values. B. The "Cell adhesion_Endothelial cell contacts by junctional mechanisms" is highlighted, with symbols representing proteins and arrows indicating protein interactions (green for activation and red for inhibition). Thermometer-like histograms visually represent microarray gene expressions, with blue indicating downregulation and red indicating upregulation.

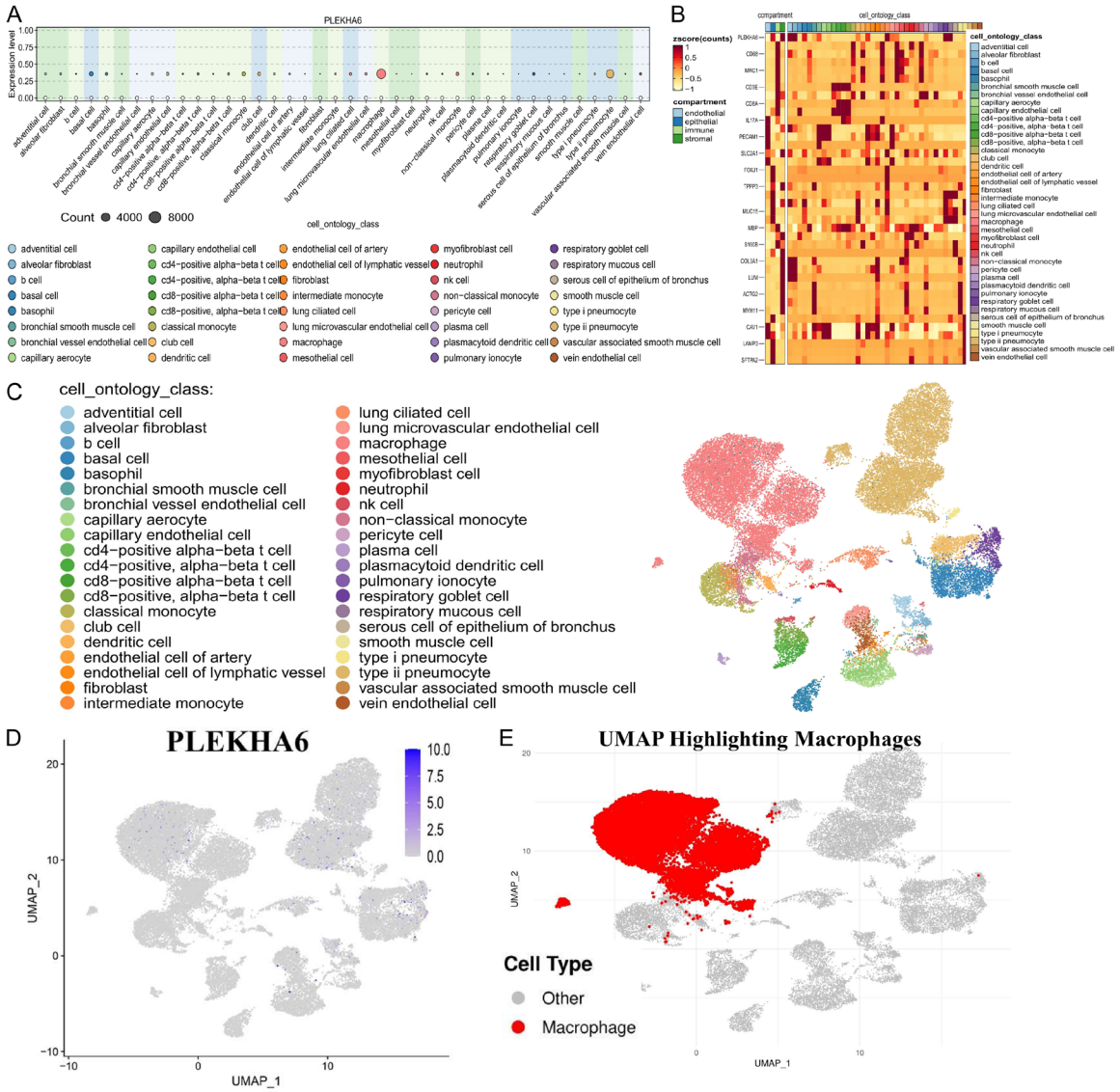

Figure 8. Single-cell transcriptomic analysis of PLEKHA6 expression and macrophage association. A. Dot plot showing PLEKHA6 expression across cell types; dot size indicates the percentage of expressing cells, and color reflects expression level. B. Heatmap of gene expression across cell ontology classes, with PLEKHA6 highlighted. C. UMAP plot showing clustering of single cells by annotated cell type. D. Feature plot displaying PLEKHA6 expression levels across the UMAP landscape. E. UMAP highlighting macrophages (blue), indicating spatial association with PLEKHA6-expressing clusters. Macrophages highlighted in blue, showing the spatial distribution of macrophages relative to other cell types and suggesting a potential association between PLEKHA6 expression and macrophage-enriched regions.

known to promote immune suppression and cancer cell survival under hostile conditions [52, 60, 61].

To further dissect this association, we extended our UMAP-based analysis to incorporate major immune lineages including $CD4^+$ and $CD8^+$ T cells, B cells, NK cells, dendritic cells, and monocytes, alongside macrophages (**Figure 8E**). This expanded mapping revealed that PLEKHA6 expression remained highly restricted to macrophage populations, with minimal co-expression in other immune subsets, underscoring its specificity. To validate functional implications, we analyzed the co-expression of PLEKHA6 with markers of immunosuppressive macrophage phenotypes (CD163, MRC1, IL10), which were positively correlated in macrophage-enriched clusters (Supplementary Figure 6). These data suggest that PLEKHA6 may con-

tribute to shaping TAM function and polarization within the LUAD microenvironment, potentially fostering an immune-evasive, tumor-promoting niche. The preferential localization of PLEKHA6 in macrophages, particularly M2-like TAMs, highlights its potential as a molecular target for disrupting pro-tumor immune remodeling in LUAD.

Association between PLEKHA6 and drug sensitivity in LUAD

To assess the therapeutic potential of PLEKHA6 in LUAD, we correlated its expression with drug response using the GDSC and CTRP pharmacogenomic datasets. High PLEKHA6 expression was strongly associated with increased sensitivity to Austocystin D and Foretinib (**Figure 9A**, **9B**). Austocystin D, a mycotoxin with anti-cancer activity, may exert selective efficacy in PLEKHA6-high LUAD cells by antagonizing redox imbalance and β-catenin-driven oncogenic signaling. Given that PLEKHA6 enhances β-catenin activation, this suggests that Austocystin D could disrupt mitochondrial or cytoskeletal functions maintained by PLEKHA6 overexpression [62]. Foretinib, a multi-kinase inhibitor targeting MET, VEGFR2, and RON, also showed pronounced efficacy in PLEKHA6-high cell lines. This aligns with our pathway analysis, which revealed that PLEKHA6 modulates Ephrin-B signaling, cadherin-mediated adhesion, and Rho GTPase-driven cytoskeletal remodeling - networks that converge on MET and VEGF signaling. Foretinib's disruption of these pathways may impair the survival and migratory advantages conferred by PLEKHA6 [63, 64].

To probe potential direct interactions, molecular docking simulations using the AlphaFold-predicted PLEKHA6 structure identified Pocket 6 as a druggable site (**Figure 9C-F**). Both Austocystin D and Foretinib displayed strong binding affinities and stable interactions within this region (**Figure 9C-F**). Austocystin D engaged in multiple hydrogen bonds and hydrophobic contacts, while Foretinib formed polar interactions near the pleckstrin homology domain, supporting their potential to modulate PLEKHA6 activity directly. These findings reveal that PLEKHA6 expression stratifies LUAD cells by drug sensitivity and may represent a biomarker for therapeutic response. The convergence of transcriptomic association and structural binding evidence positions PLEKHA6 as a promising candidate for targeted therapy or biomarker-guided drug repurposing in LUAD.

Biological functions of PLEKHA6 in LUAD cells

To experimentally validate the functional role of PLEKHA6 in LUAD, we generated A549 cell lines stably expressing two independent shRNAs targeting PLEKHA6 (shPLEKHA6#1 and shPLEKHA6#2). Knockdown efficiency was confirmed by RT-qPCR and Western blot, both showing a significant reduction in PLEKHA6 expression compared to shLacZ control cells (**Figure 10A-G**). Western blot analysis further demonstrated a marked decrease in β-catenin protein levels in PLEKHA6-silenced cells, suggesting that PLEKHA6 may serve as an upstream regulator of the Wnt/β-catenin signaling pathway. In addition, we observed a concomitant reduction in VE-cadherin expression, a key adherens junction molecule that anchors β-catenin at the cell membrane. β-catenin and VE-cadherin are functionally interconnected components of the adherens junction complex, where VE-cadherin anchors β-catenin at the plasma membrane and regulates its stability. This interaction is crucial for maintaining epithelial architecture and modulating downstream Wnt signaling. Our observation that PLEKHA6 knockdown leads to concurrent downregulation of both β-catenin and VE-cadherin supports the hypothesis that PLEKHA6 contributes to LUAD progression by stabilizing this complex. Loss of this regulatory axis may not only weaken intercellular adhesion but also impair β-catenin's transcriptional activity, ultimately reducing proliferative and migratory potential. β-catenin is a pivotal effector of the canonical Wnt pathway, which regulates proliferation, stemness, and cell migration in various cancers, including LUAD. The suppression of β-catenin upon PLEKHA6 knockdown aligns with our transcriptomic and MetaCore pathway enrichment results, which implicated PLEKHA6 in key oncogenic networks such as Ephrin-B signaling, Rho GTPase-mediated cytoskeletal remodeling, and classical cadherin-mediated adhesion pathways that converge on or influence β-catenin stability and activity. These findings suggest that PLEKHA6 may act as a positive regulator of β-catenin, potentially by stabilizing it at the membrane or influencing its cytoskeletal transport and nuclear translocation. Given that aberrant activation of β-catenin promotes EMT, proliferation, and resistance in

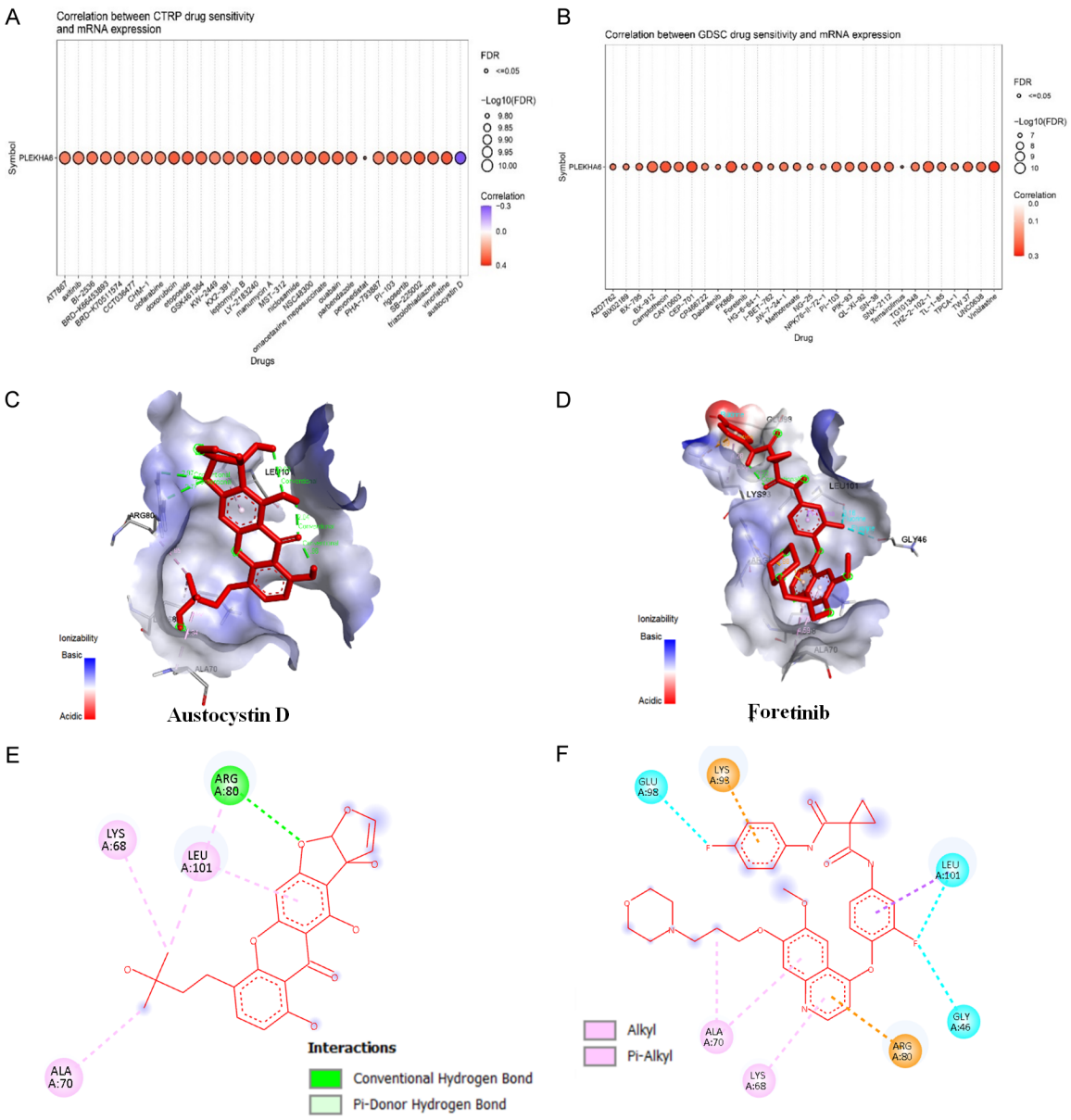

Figure 9. Correlation analysis and molecular docking of PLEKHA6 with potential drugs. A. Correlation between PLEKHA6 mRNA expression and drug sensitivity in the GDSC database. Significant positive correlations are highlighted in red. B. Correlation between PLEKHA6 expression and drug response in the CTRP database, with Austocystin D identified as a significantly associated compound. C. Predicted docking poses of Austocystin D bound to PLEKHA6, showing the interaction site. D. 2D interaction diagram of Austocystin D with PLEKHA6, indicating key interacting amino acid residues. E. Predicted docking pose of Foretinib with the PLEKHA6 protein, illustrating its position within the binding pocket. F. 2D interaction diagram of Foretinib and PLEKHA6, displaying hydrogen bonding and hydrophobic interactions.

LUAD, our data highlight PLEKHA6 as a potential upstream effector in this oncogenic axis. Targeting PLEKHA6 may thus offer a means to suppress Wnt-driven tumor progression. These insights support the emerging view that pleckstrin homology domain-containing proteins participate in scaffolding or trafficking mechanisms critical for oncogenic signaling [65-68].

Functional impact of PLEKHA6 in LUAD cells

To determine the phenotypic impact of PLEKHA6 knockdown, we performed a series of functional assays using shPLEKHA6#1 and shPLEKHA6#2 A549 cell lines. Cell proliferation assessed via MTT assay at 0, 24, 48, and 72 hours, showed significantly reduced viability

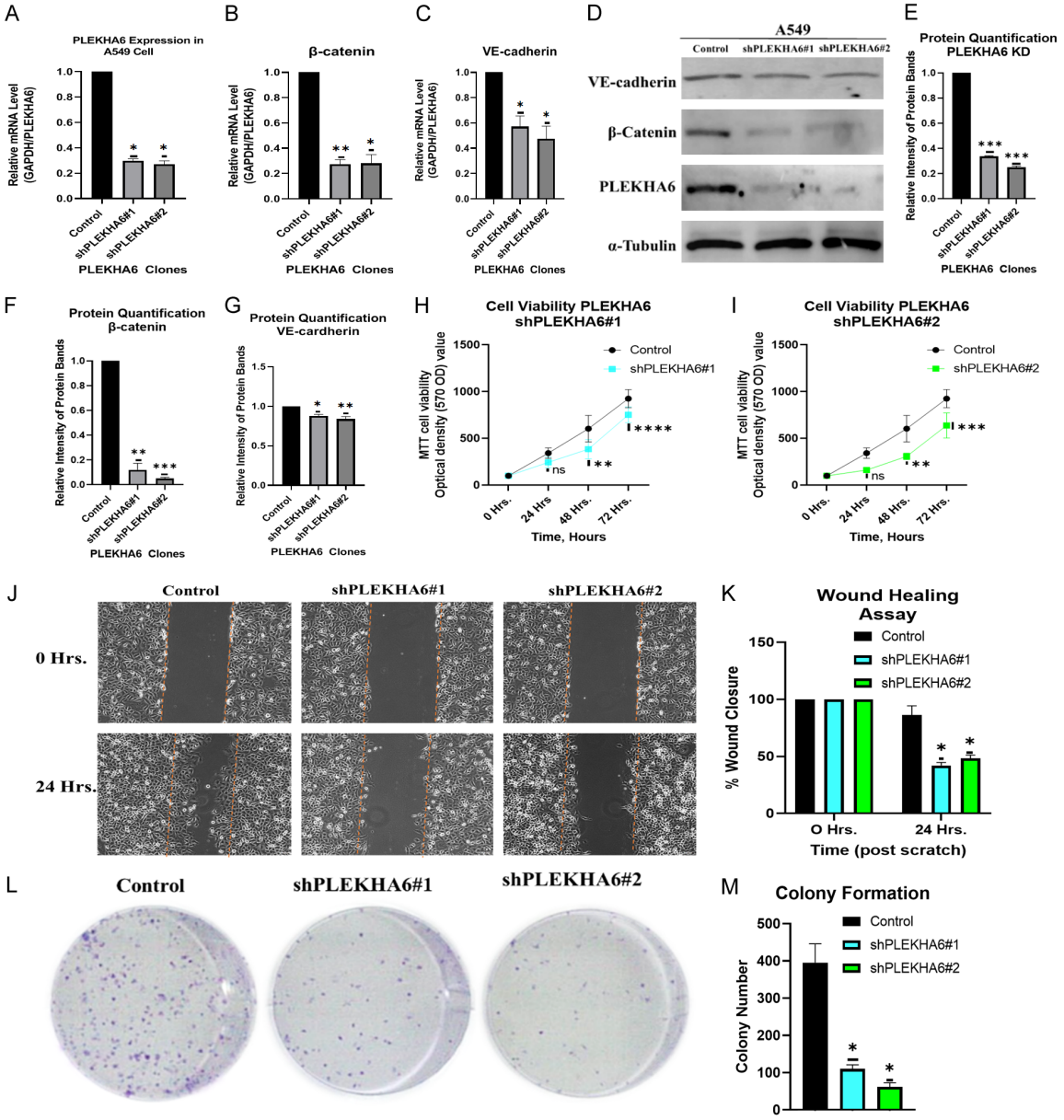

Figure 10. PLEKHA6 knockdown impairs expression, viability, migration, and clonogenic potential of A549 cells. (A-C) RT-qPCR validation of PLEKHA6 knockdown in A549 cells transduced with shPLEKHA6#1 and shPLEKHA6#2 compared to shLacZ control. (D) Western blot confirming reduced PLEKHA6 protein levels in knockdown cells; α-tubulin, was used as the loading control. (E-G) Densitometric analysis of Western blot bands, normalized to α-tubulin, quantifying knockdown efficiency. (H, I) MTT assay showing significantly decreased cell viability in PLEKHA6-depleted cells over 72 hours. Data are presented as mean ± SD; $P < 0.01$. (J, K) Wound healing assay demonstrating reduced migration in PLEKHA6 knockdown cells. (H) Representative images and (I) quantitative analysis after 24 hours. (L, M) Colony formation assay. (L) Representative images of colony formation. (M) Quantification showing reduced colony number and size in knockdown cells.

in PLEKHA6-deficient cells compared to the shLacZ control (**Figure 10H**, **10I**). This reduction is consistent with impaired β-catenin signaling, which is known to regulate cell cycle progression via transcriptional activation of targets such as c-Myc and Cyclin D1 [67]. Wound-healing assays demonstrated a marked delay in migration in PLEKHA6-silenced cells (**Figure 10J**, **10K**), suggesting compromised motility, possibly due to cytoskeletal disorganization mediated by the Rho GTPase pathway another node highlighted in our MetaCore analysis.

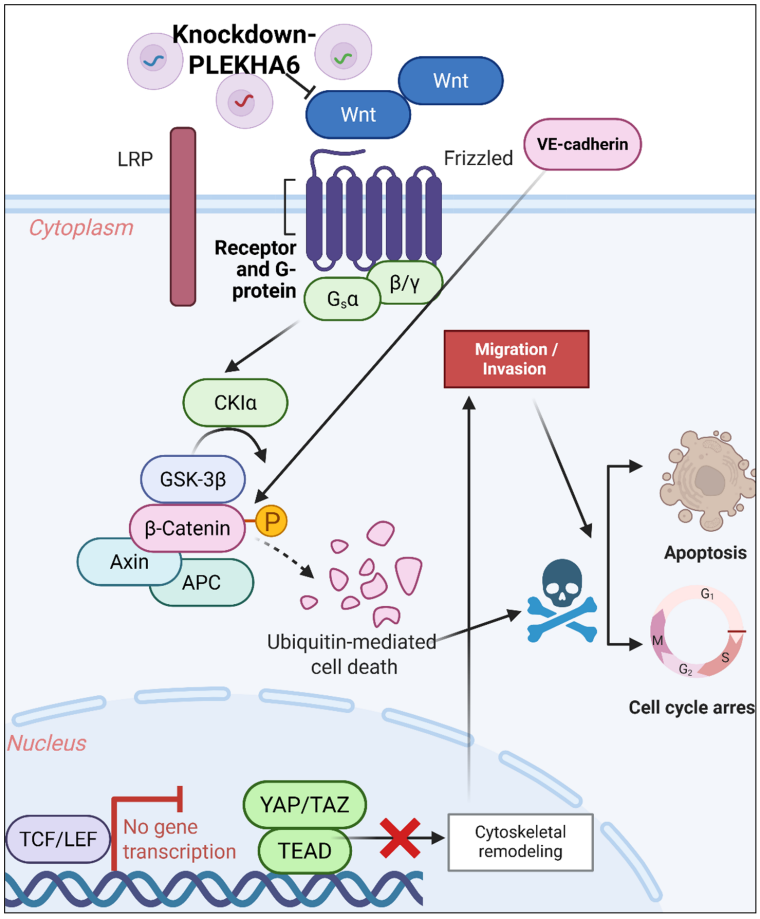

Figure 11. Schematic representation of the molecular mechanisms regulated by PLEKHA6 in LUAD. Knockdown of PLEKHA6 (KD-PLEKHA6) inhibits Wnt signaling by promoting β-catenin degradation through the destruction complex (Axin, APC, GSK-3β, CKIα), leading to reduced TCF/LEF-mediated transcription and resulting in apoptosis and cell cycle arrest.

Additionally, colony formation assays revealed that PLEKHA6 knockdown significantly impaired the clonogenic potential of A549 cells (**Figure 10L**, **10M**), further supporting a role for PLEKHA6 in sustaining tumorigenic properties. Together, these results confirm that PLEKHA6 contributes to multiple hallmarks of LUAD, including proliferation, migration, and self-renewal. The coordinated suppression of these phenotypes upon PLEKHA6 knockdown alongside reduced β-catenin levels supports its role as a potential therapeutic target and prognostic biomarker in LUAD. Considering the clinical correlation between elevated PLEKHA6 expression and poor survival outcomes, this gene warrants further exploration for integration into Wnt-pathway-targeted or combination therapies.

Discussion

LUAD remains a major clinical challenge due to late diagnosis, high metastatic potential, and therapy resistance [62]. This study identifies PLEKHA6, a pleckstrin homology (PH) domain-containing protein, as a novel biomarker and regulator of LUAD progression. Through integrative multi-omics analysis - including transcriptomics, single-cell profiling, DNA methylation, protein expression, molecular docking, and functional validation, we demonstrate that PLEKHA6 is overexpressed in LUAD and associated with poor prognosis, pro-tumor immune polarization, and potential drug sensitivity. PH domain - containing proteins play key roles in cytoskeletal dynamics, signaling transduction, and vesicular trafficking [69-72]. In cancer, several members - such as PLEKHA7, have been shown to influence epithelial integrity and metastasis [73, 74]. Here, we show that PLEKHA6 promotes LUAD proliferation and migration, partly through stabilizing VE-ca-dherin/β-catenin complexes and facilitating Wnt signaling, a canonical pathway in LUAD tumorigenesis. Knockdown of PLEKHA6 downregulates β-catenin and suppresses oncogenic phenotypes in A549 cells, supporting its role as a positive regulator of LUAD aggressiveness.

Importantly, single-cell RNA-seq analysis revealed PLEKHA6 to be enriched in TAMs, particularly those exhibiting immunosuppressive (M2-like) phenotypes. Co-expression of PLEKHA6 with CD163, MRC1, and IL10 reinforces its potential role in shaping the immunosuppressive tumor TME. This is supported by prior findings involving PLEKHA4, which was shown to correlate with M2 macrophage infiltration in glioma [75, 76]. This macrophage-specific pattern, with limited expression in cytotoxic $CD8^+$ T cells and NK cells, suggests that PLEKHA6 may

contribute to immune evasion by reinforcing TAM polarization [77, 78].

Therapeutically, drug sensitivity profiling and molecular docking highlighted Austocystin D and Foretinib as potential agents for targeting PLEKHA6-expressing LUAD cells. Foretinib, in particular, targets MET and VEGFR2 pathways, which intersect with the cytoskeletal remodeling and cadherin-mediated adhesion networks enriched in PLEKHA6-high LUAD. Its high binding affinity for a predicted PLEKHA6 functional pocket further supports the feasibility of direct pharmacological inhibition. These findings provide a molecular basis for further preclinical validation of PLEKHA6-targeted therapies, particularly in patients with high PLEKHA6 expression. In the other hand, our *in vitro* experiments offer strong functional support for the oncogenic role of PLEKHA6. Knockdown of PLEKHA6 in LUAD cells led to reduced expression of β-catenin at both the transcript and protein levels, as well as decreased proliferation, migration, and clonogenic growth. These effects are consistent with disruption of Wnt/β-catenin signaling, a critical pathway in LUAD pathogenesis and therapeutic resistance.

Conclusion

In conclusion, our study provides a comprehensive characterization of PLEKHA6 as a key oncogenic driver and immune modulator in LUAD. Through integrative omics and experimental validation, we identify PLEKHA6 as a novel biomarker and targetable protein, offering opportunities for both diagnostic development and personalized therapeutic strategies in LUAD (**Figure 11**).

Acknowledgements

This study was supported by a grant from the Wan Fang Hospital (114TMU-WFH-14), Shin Kong Wu Ho-Su Memorial Hospital (SKH-TMU-113-06 and SKH-TMU-114-03), Shuang-Ho Hospital (W113YSR_03 and W114FRP-18) and National Science and Technology Council under the Grants (NSTC 114-2314-B-038-152, and NSTC114-2314-B-038-133-MY3), as well as the "TMU Research Center of Cancer Translational Medicine" from The Featured Areas Research Center Program within the framework of the Higher Education Sprout Project by the Ministry of Education (MOE) in Taiwan. The authors thank the statistical/computational/technical support of the Clinical Data Center, Office of Data Science, Taipei Medical University, Taiwan. We thank the RNA Technology Platform and Gene Manipulation Core Facility (RNAi core) of the National Core Facility for Biopharmaceuticals at Academia Sinica (Taipei, Taiwan) for providing related shRNA and CRISPR services.

Disclosure of conflict of interest

None.

Abbreviations

LUAD, Lung Adenocarcinoma; NSCLC, Non-Small Cell Lung Cancer; PLEKHA6, Pleckstrin Homology Domain Containing A6; TME, Tumor Microenvironment; TAMs, Tumor-Associated Macrophages; scRNA-seq, Single-Cell RNA Sequencing; PFI, Progression-Free Interval; PPI, Protein-Protein Interaction; TCGA, The Cancer Genome Atlas; GEO, Gene Expression Omnibus; GTEx, Genotype-Tissue Expression; CCLE, Cancer Cell Line Encyclopedia; UMAP, Uniform Manifold Approximation and Projection; PH domain, Pleckstrin Homology Domain; UMI, Unique Molecular Identifier; PCA, Principal Component Analysis; RT-qPCR, Reverse Transcription Quantitative Polymerase Chain Reaction; shRNA, Short Hairpin RNA; VE-cadherin, Vascular Endothelial Cadherin; CTRPs, Cancer Therapeutics Response Portals; GSCA, Genomics of Drug Sensitivity in Cancer Analysis.

Address correspondence to: Chih-Yang Wang, Graduate Institute of Cancer Biology and Drug Discovery, College of Medical Science and Technology, Taipei Medical University, Taipei 11031, Taiwan. E-mail: chihyang@tmu.edu.tw; Ming-Cheng Tsai, School of Medicine, Fu Jen Catholic University, New Taipei City 242, Taiwan. E-mail: m000679@yahoo.com.tw

References

[1] Siegel RL, Kratzer TB, Giaquinto AN, Sung H and Jemal A. Cancer statistics, 2025. CA Cancer J Clin 2025; 75: 10-45.

[2] Collins LG, Haines C, Perkel R and Enck RE. Lung cancer: diagnosis and management. Am Fam Physician 2007; 75: 56-63.

[3] Chung CC, Huang TY, Chu HR, De Luca R, Candelotti E, Huang CH, Yang YSH, Incerpi S, Pedersen JZ, Lin CY, Huang HM, Lee SY, Li ZL, ChangOu CA, Li WS, Davis PJ, Lin HY, Whang-Peng J and Wang K. Heteronemin and tetrac derivatives suppress non-small cell lung cancer

growth via ERK1/2 inhibition. Food Chem Toxicol 2022; 161: 112850.
[4] Hsiao SH, Chen WT, Chung CL, Chou YT, Lin SE, Hong SY, Chang JH, Chang TH and Chien LN. Comparative survival analysis of platinum-based adjuvant chemotherapy for early-stage squamous cell carcinoma and adenocarcinoma of the lung. Cancer Med 2022; 11: 2067-2078.
[5] Kuo KT, Lin CH, Wang CH, Pikatan NW, Yadav VK, Fong IH, Yeh CT, Lee WH and Huang WC. HNMT upregulation induces cancer stem cell formation and confers protection against oxidative stress through interaction with HER2 in non-small-cell lung cancer. Int J Mol Sci 2022; 23: 1663.
[6] Tseng PC, Chen CL, Lee KY, Feng PH, Wang YC, Satria RD and Lin CF. Epithelial-to-mesenchymal transition hinders interferon-γ-dependent immunosurveillance in lung cancer cells. Cancer Lett 2022; 539: 215712.
[7] Lee HC, Lu YH, Huang YL, Huang SL and Chuang HC. Air pollution effects to the subtype and severity of lung cancers. Front Med (Lausanne) 2022; 9: 835026.
[8] Spella M and Stathopoulos GT. Immune resistance in lung adenocarcinoma. Cancers (Basel) 2021; 13: 384.
[9] Tsai HE, Liu GS, Kung ML, Liu LF, Wu JC, Tang CH, Huang CH, Chen SC, Lam HC, Wu CS and Tai MH. Downregulation of hepatoma-derived growth factor contributes to retarded lung metastasis via inhibition of epithelial-mesenchymal transition by systemic POMC gene delivery in melanoma. Mol Cancer Ther 2013; 12: 1016-1025.
[10] Tsai HE, Liu LF, Dusting GJ, Weng WT, Chen SC, Kung ML, Tee R, Liu GS and Tai MH. Pro-opiomelanocortin gene delivery suppresses the growth of established Lewis lung carcinoma through a melanocortin-1 receptor-independent pathway. J Gene Med 2012; 14: 44-53.
[11] Yamada K, Nomura N, Yamano A, Yamada Y and Wakamatsu N. Identification and characterization of splicing variants of PLEKHA5 (Plekha5) during brain development. Gene 2012; 492: 270-275.
[12] Powis G, Meuillet EJ, Indarte M, Booher G and Kirkpatrick L. Pleckstrin Homology [PH] domain, structure, mechanism, and contribution to human disease. Biomed Pharmacother 2023; 165: 115024.
[13] Xing X, Mu N, Yuan X, Wang N, Juhlin CC, Stråat K, Larsson C and Xu D. PLEKHS1 over-expression is associated with metastases and poor outcomes in papillary thyroid carcinoma. Cancers (Basel) 2020; 12: 2133.
[14] Jeung HC, Puentes R, Aleshin A, Indarte M, Correa RG, Bankston LA, Layng FIAL, Ahmed Z, Wistuba I, Yao Y, Duenas DG, Zhang S, Meuillet EJ, Marassi F, Liddington RC, Kirkpatrick L and Powis G. PLEKHA7 signaling is necessary for the growth of mutant KRAS driven colorectal cancer. Exp Cell Res 2021; 409: 112930.
[15] Nagamura Y, Miyazaki M, Nagano Y, Yuki M, Fukami K, Yanagihara K, Sasaki K, Sakai R and Yamaguchi H. PLEKHA5 regulates the survival and peritoneal dissemination of diffuse-type gastric carcinoma cells with Met gene amplification. Oncogenesis 2021; 10: 25.
[16] GTEx Consortium. The genotype-tissue expression (GTEx) project. Nat Genet 2013; 45: 580-585.
[17] Reimand J, Arak T, Adler P, Kolberg L, Reisberg S, Peterson H and Vilo J. g:Profiler-a web server for functional interpretation of gene lists (2016 update). Nucleic Acids Res 2016; 44: W83-W89.
[18] Akhmedov M, Martinelli A, Geiger R and Kwee I. Omics playground: a comprehensive self-service platform for visualization, analytics and exploration of big omics data. NAR Genom Bioinform 2019; 2: lqz019.
[19] Tang D, Chen M, Huang X, Zhang G, Zeng L, Zhang G, Wu S and Wang Y. SRplot: a free online platform for data visualization and graphing. PLoS One 2023; 18: e0294236.
[20] Chen YL, Lee KT, Wang CY, Shen CH, Chen SC, Chung WP, Hsu YT, Kuo YL, Chen PS, Cheung CHA, Chang CP, Shen MR and Hsu HP. Low expression of cytosolic NOTCH1 predicts poor prognosis of breast cancer patients. Am J Cancer Res 2022; 12: 2084-2101.
[21] Li CY, Anuraga G, Chang CP, Weng TY, Hsu HP, Ta HDK, Su PF, Chiu PH, Yang SJ, Chen FW, Ye PH, Wang CY and Lai MD. Repurposing nitric oxide donating drugs in cancer therapy through immune modulation. J Exp Clin Cancer Res 2023; 42: 22.
[22] Hagerling C, Gonzalez H, Salari K, Wang CY, Lin C, Robles I, van Gogh M, Dejmek A, Jirström K and Werb Z. Immune effector monocyte-neutrophil cooperation induced by the primary tumor prevents metastatic progression of breast cancer. Proc Natl Acad Sci U S A 2019; 116: 21704-21714.
[23] Tang Z, Kang B, Li C, Chen T and Zhang Z. GEPIA2: an enhanced web server for large-scale expression profiling and interactive analysis. Nucleic Acids Res 2019; 47: W556-W560.
[24] Chandrashekar DS, Karthikeyan SK, Korla PK, Patel H, Shovon AR, Athar M, Netto GJ, Qin ZS, Kumar S, Manne U, Creighton CJ and Varambally S. UALCAN: an update to the integrated cancer data analysis platform. Neoplasia 2022; 25: 18-27.
[25] Xuan DTM, Wu CC, Wang WJ, Hsu HP, Ta HDK, Anuraga G, Chiao CC and Wang CY. Glutamine synthetase regulates the immune microenvironment and cancer development through the

inflammatory pathway. Int J Med Sci 2023; 20: 35-49.
[26] Chandrashekar DS, Bashel B, Balasubramanya SAH, Creighton CJ, Ponce-Rodriguez I, Chakravarthi BVSK and Varambally S. UALCAN: a portal for facilitating tumor subgroup gene expression and survival analyses. Neoplasia 2017; 19: 649-658.
[27] Chiao CC, Liu YH, Phan NN, An Ton NT, Ta HDK, Anuraga G, Minh Xuan DT, Fitriani F, Putri Hermanto EM, Athoillah M, Andriani V, Ajiningrum PS, Wu YF, Lee KH, Chuang JY, Wang CY and Kao TJ. Prognostic and genomic analysis of proteasome 20S subunit alpha (PSMA) family members in breast cancer. Diagnostics (Basel) 2021; 11: 2220.
[28] Wang CY, Chao YJ, Chen YL, Wang TW, Phan NN, Hsu HP, Shan YS and Lai MD. Upregulation of peroxisome proliferator-activated receptor-α and the lipid metabolism pathway promotes carcinogenesis of ampullary cancer. Int J Med Sci 2021; 18: 256-269.
[29] Modhukur V, Iljasenko T, Metsalu T, Lokk K, Laisk-Podar T and Vilo J. MethSurv: a web tool to perform multivariable survival analysis using DNA methylation data. Epigenomics 2018; 10: 277-288.
[30] Wang CY, Chiao CC, Phan NN, Li CY, Sun ZD, Jiang JZ, Hung JH, Chen YL, Yen MC, Weng TY, Chen WC, Hsu HP and Lai MD. Gene signatures and potential therapeutic targets of amino acid metabolism in estrogen receptor-positive breast cancer. Am J Cancer Res 2020; 10: 95-113.
[31] Kao TJ, Wu CC, Phan NN, Liu YH, Ta HDK, Anuraga G, Wu YF, Lee KH, Chuang JY and Wang CY. Prognoses and genomic analyses of proteasome 26S subunit, ATPase (PSMC) family genes in clinical breast cancer. Aging (Albany NY) 2021; 13: 17970.
[32] Ghandi M, Huang FW, Jané-Valbuena J, Kryukov GV, Lo CC, McDonald ER 3rd, Barretina J, Gelfand ET, Bielski CM, Li H, Hu K, Andreev-Drakhlin AY, Kim J, Hess JM, Haas BJ, Aguet F, Weir BA, Rothberg MV, Paolella BR, Lawrence MS, Akbani R, Lu Y, Tiv HL, Gokhale PC, de Weck A, Mansour AA, Oh C, Shih J, Hadi K, Rosen Y, Bistline J, Venkatesan K, Reddy A, Sonkin D, Liu M, Lehar J, Korn JM, Porter DA, Jones MD, Golji J, Caponigro G, Taylor JE, Dunning CM, Creech AL, Warren AC, McFarland JM, Zamanighomi M, Kauffmann A, Stransky N, Imielinski M, Maruvka YE, Cherniack AD, Tsherniak A, Vazquez F, Jaffe JD, Lane AA, Weinstock DM, Johannessen CM, Morrissey MP, Stegmeier F, Schlegel R, Hahn WC, Getz G, Mills GB, Boehm JS, Golub TR, Garraway LA and Sellers WR. Next-generation characterization of the cancer cell line encyclopedia. Nature 2019; 569: 503-508.
[33] Hsieh YY, Du JL and Yang PM. Repositioning VU-0365114 as a novel microtubule-destabilizing agent for treating cancer and overcoming drug resistance. Mol Oncol 2024; 18: 386-414.
[34] Ko CC, Hsieh YY and Yang PM. Long non-coding RNA MIR31HG promotes the transforming growth factor β-induced epithelial-mesenchymal transition in pancreatic ductal adenocarcinoma cells. Int J Mol Sci 2022; 23: 6559.
[35] Lin JC, Liu TP, Chen YB, Huang TS, Chen TY and Yang PM. Inhibition of CDK9 exhibits anticancer activity in hepatocellular carcinoma cells via targeting ribonucleotide reductase. Toxicol Appl Pharmacol 2023; 471: 116568.
[36] Yang PM, Hong YH, Hsu KC and Liu TP. p38α/S1P/SREBP2 activation by the SAM-competitive EZH2 inhibitor GSK343 limits its anticancer activity but creates a druggable vulnerability in hepatocellular carcinoma. Am J Cancer Res 2019; 9: 2120-2139.
[37] Yang W, Soares J, Greninger P, Edelman EJ, Lightfoot H, Forbes S, Bindal N, Beare D, Smith JA, Thompson IR, Ramaswamy S, Futreal PA, Haber DA, Stratton MR, Benes C, McDermott U and Garnett MJ. Genomics of drug sensitivity in cancer (GDSC): a resource for therapeutic biomarker discovery in cancer cells. Nucleic Acids Res 2013; 41: D955-D961.
[38] Fleming J, Magaña P, Nair S, Tsenkov M, Bertoni D, Pidruchna I, Lima Afonso MQ, Midlik A, Paramval U, Žídek A, Laydon A, Kovalevskiy O, Pan J, Cheng J, Avsec Ž, Bycroft C, Wong LH, Last M, Mirdita M, Steinegger M, Kohli P, Váradi M and Velankar S. Alphafold protein structure database and 3D-beacons: new data and capabilities. J Mol Biol 2025; 437: 168967.
[39] Huey R, Morris GM and Forli S. Using autodock 4 and autodock vina with autodocktools: a tutorial. The Scripps Research Institute Molecular Graphics Laboratory 2012; 10550: 1000.
[40] Yuan S, Chan HS and Hu Z. Using PyMOL as a platform for computational drug design. Wiley Interdisciplinary Reviews: Computational Molecular Science 2017; 7: e1298.
[41] Yuan S, Chan HCS, Filipek S and Vogel H. PyMOL and inkscape bridge the data and the data visualization. Structure 2016; 12: 2041-2042.
[42] Szklarczyk D, Franceschini A, Wyder S, Forslund K, Heller D, Huerta-Cepas J, Simonovic M, Roth A, Santos A, Tsafou KP, Kuhn M, Bork P, Jensen LJ and von Mering C. STRING v10: protein-protein interaction networks, integrated over the tree of life. Nucleic Acids Res 2015; 43: D447-D452.
[43] Shannon P, Markiel A, Ozier O, Baliga NS, Wang JT, Ramage D, Amin N, Schwikowski B and Ideker T. Cytoscape: a software environment for integrated models of biomolecular

interaction networks. Genome Res 2003; 13: 2498-2504.
[44] Xuan DTM, Yeh IJ, Wu CC, Su CY, Liu HL, Chiao CC, Ku SC, Jiang JZ, Sun Z, Ta HDK, Anuraga G, Wang CY and Yen MC. Comparison of transcriptomic signatures between monkeypox-infected monkey and human cell lines. J Immunol Res 2022; 2022: 3883822.
[45] Anuraga G, Wang WJ, Phan NN, An Ton NT, Ta HDK, Berenice Prayugo F, Minh Xuan DT, Ku SC, Wu YF, Andriani V, Athoillah M, Lee KH and Wang CY. Potential prognostic biomarkers of NIMA (never in mitosis, gene A)-related kinase (NEK) family members in breast cancer. J Pers Med 2021; 11: 1089.
[46] Ta HDK, Wang WJ, Phan NN, An Ton NT, Anuraga G, Ku SC, Wu YF, Wang CY and Lee KH. Potential therapeutic and prognostic values of LSM family genes in breast cancer. Cancers (Basel) 2021; 13: 4902.
[47] Tabula Sapiens Consortium*; Jones RC, Karkanias J, Krasnow MA, Pisco AO, Quake SR, Salzman J, Yosef N, Bulthaup B, Brown P, Harper W, Hemenez M, Ponnusamy R, Salehi A, Sanagavarapu BA, Spallino E, Aaron KA, Concepcion W, Gardner JM, Kelly B, Neidlinger N, Wang Z, Crasta S, Kolluru S, Morri M, Tan SY, Travaglini KJ, Xu C, Alcántara-Hernández M, Almanzar N, Antony J, Beyersdorf B, Burhan D, Calcuttawala K, Carter MM, Chan CKF, Chang CA, Chang S, Colville A, Culver RN, Cvijović I, D'Amato G, Ezran C, Galdos FX, Gillich A, Goodyer WR, Hang Y, Hayashi A, Houshdaran S, Huang X, Irwin JC, Jang S, Juanico JV, Kershner AM, Kim S, Kiss B, Kong W, Kumar ME, Kuo AH, Li B, Loeb GB, Lu WJ, Mantri S, Markovic M, McAlpine PL, de Morree A, Mrouj K, Mukherjee S, Muser T, Neuhöfer P, Nguyen TD, Perez K, Puluca N, Qi Z, Rao P, Raquer-McKay H, Schaum N, Scott B, Seddighzadeh B, Segal J, Sen S, Sikandar S, Spencer SP, Steffes LC, Subramaniam VR, Swarup A, Swift M, Van Treuren W, Trimm E, Veizades S, Vijayakumar S, Vo KC, Vorperian SK, Wang W, Weinstein HNW, Winkler J, Wu TTH, Xie J, Yung AR, Zhang Y, Detweiler AM, Mekonen H, Neff NF, Sit RV, Tan M, Yan J, Bean GR, Charu V, Forgó E, Martin BA, Ozawa MG, Silva O, Toland A, Vemuri VNP, Afik S, Awayan K, Botvinnik OB, Byrne A, Chen M, Dehghannasiri R, Gayoso A, Granados AA, Li Q, Mahmoudabadi G, McGeever A, Olivieri JE, Park M, Ravikumar N, Stanley G, Tan W, Tarashansky AJ, Vanheusden R, Wang P, Wang S, Xing G, Dethlefsen L, Ezran C, Gillich A, Hang Y, Ho PY, Irwin JC, Jang S, Leylek R, Liu S, Maltzman JS, Metzger RJ, Phansalkar R, Sasagawa K, Sinha R, Song H, Swarup A, Trimm E, Veizades S, Wang B, Beachy PA, Clarke MF, Giudice LC, Huang FW, Huang KC, Idoyaga J, Kim SK, Kuo CS, Nguyen P, Rando TA, Red-Horse K, Reiter J, Relman DA, Sonnenburg JL, Wu A, Wu SM and Wyss-Coray T. The tabula sapiens: a multiple-organ, single-cell transcriptomic atlas of humans. Science 2022; 376: eabl4896.
[48] Cakir B, Prete M, Huang N, Van Dongen S, Pir P and Kiselev VY. Comparison of visualization tools for single-cell RNAseq data. NAR Genom Bioinform 2020; 2: lqaa052.
[49] Hao Y, Stuart T, Kowalski MH, Choudhary S, Hoffman P, Hartman A, Srivastava A, Molla G, Madad S, Fernandez-Granda C and Satija R. Dictionary learning for integrative, multimodal and scalable single-cell analysis. Nat Biotechnol 2024; 42: 293-304.
[50] Gu Z, Eils R and Schlesner M. Complex heatmaps reveal patterns and correlations in multidimensional genomic data. Bioinformatics 2016; 32: 2847-2849.
[51] Chen CL, Tseng PC, Chao YP, Shen TJ, Jhan MK, Wang YT, Nguyen TT and Lin CF. Polypeptide antibiotic actinomycin D induces Mcl-1 uncanonical downregulation in lung cancer cell apoptosis. Life Sci 2023; 321: 121615.
[52] Kumar S, Wu CC, Wulandari FS, Chiao CC, Ko CC, Lin HY, Ngadio JL, Rebecca C, Xuan DTM, Solomon DD, Michael M, Kristiani L, Chuang JY, Tsai MC and Wang CY. Integration of multi-omics and single-cell transcriptome reveals mitochondrial outer membrane protein-2 (MTX-2) as a prognostic biomarker and characterizes ubiquinone metabolism in lung adenocarcinoma. J Cancer 2025; 16: 2401-2420.
[53] Wu YJ, Chiao CC, Chuang PK, Hsieh CB, Ko CY, Ko CC, Chang CF, Chen TY, Nguyen NUN, Hsu CC, Chu TH, Fang CC, Tsai HY, Tsai HC, Anuraga G, Ta HDK, Xuan DTM, Kumar S, Dey S, Wulandari FS, Manalu RT, Ly NP, Wang CY and Lee YK. Comprehensive analysis of bulk and single-cell RNA sequencing data reveals Schlafen-5 (SLFN5) as a novel prognosis and immunity. Int J Med Sci 2024; 21: 2348-2364.
[54] Xuan DTM, Yeh IJ, Liu HL, Su CY, Ko CC, Ta HDK, Jiang JZ, Sun Z, Lin HY, Wang CY and Yen MC. A comparative analysis of Marburg virus-infected bat and human models from public high-throughput sequencing data. Int J Med Sci 2025; 22: 1-16.
[55] Anuraga G, Lang J, Xuan DTM, Ta HDK, Jiang JZ, Sun Z, Dey S, Kumar S, Singh A, Kajla G, Wang WJ and Wang CY. Integrated bioinformatics approaches to investigate alterations in transcriptomic profiles of monkeypox infected human cell line model. J Infect Public Health 2024; 17: 60-69.
[56] Hu X, Luo K, Shi H, Yan X, Huang R, Zhao B, Zhang J, Xie D and Zhang W. Integrated 5-hydroxymethylcytosine and fragmentation signatures as enhanced biomarkers in lung cancer. Clin Epigenetics 2022; 14: 15.

[57] Zeng D, Hu Z, Yi Y, Valeria B, Shan G, Chen Z, Zhan C, Lin M, Lin Z and Wang Q. Differences in genetics and microenvironment of lung adenocarcinoma patients with or without TP53 mutation. BMC Pulm Med 2021; 21: 316.
[58] Fu J, Li Y, Li C, Tong Y, Li M and Cang S. A special prognostic indicator: tumor mutation burden combined with immune infiltrates in lung adenocarcinoma with TP53 mutation. Transl Cancer Res 2021; 10: 3963-3978.
[59] Zhang K, Qian Y, Quan X, Zhu T and Qian B. A novel signature of lipid metabolism-related gene predicts prognosis and response to immunotherapy in lung adenocarcinoma. Front Cell Dev Biol 2022; 10: 730132.
[60] Sedighzadeh SS, Khoshbin AP, Razi S, Keshavarz-Fathi M and Rezaei N. A narrative review of tumor-associated macrophages in lung cancer: regulation of macrophage polarization and therapeutic implications. Transl Lung Cancer Res 2021; 10: 1889-1916.
[61] Conway EM, Pikor LA, Kung SH, Hamilton MJ, Lam S, Lam WL and Bennewith KL. Macrophages, inflammation, and lung cancer. Am J Respir Crit Care Med 2016; 193: 116-130.
[62] Marks KM, Park ES, Arefolov A, Russo K, Ishihara K, Ring JE, Clardy J, Clarke AS and Pelish HE. The selectivity of austocystin D arises from cell-line-specific drug activation by cytochrome P450 enzymes. J Nat Prod 2011; 74: 567-573.
[63] Eder JP, Shapiro GI, Appleman LJ, Zhu AX, Miles D, Keer H, Cancilla B, Chu F, Hitchcock-Bryan S, Sherman L, McCallum S, Heath EI, Boerner SA and LoRusso PM. A phase I study of foretinib, a multi-targeted inhibitor of c-Met and vascular endothelial growth factor receptor 2. Clin Cancer Res 2010; 16: 3507-3516.
[64] Zillhardt M, Park SM, Romero IL, Sawada K, Montag A, Krausz T, Yamada SD, Peter ME and Lengyel E. Foretinib (GSK1363089), an orally available multikinase inhibitor of c-Met and VEGFR-2, blocks proliferation, induces anoikis, and impairs ovarian cancer metastasis. Clin Cancer Res 2011; 17: 4042-4051.
[65] Clevers H and Nusse R. Wnt/β-catenin signaling and disease. Cell 2012; 149: 1192-1205.
[66] Nelson WJ and Nusse R. Convergence of Wnt, ß-catenin, and cadherin pathways. Science 2004; 303: 1483-1487.
[67] Gallegos LL, Ng MR, Sowa ME, Selfors LM, White A, Zervantonakis IK, Singh P, Dhakal S, Harper JW and Brugge JS. A protein interaction map for cell-cell adhesion regulators identifies DUSP23 as a novel phosphatase for β-catenin. Sci Rep 2016; 6: 27114.
[68] Hwang JR, Chou CL, Medvar B, Knepper MA and Jung HJ. Identification of β-catenin-interacting proteins in nuclear fractions of native rat collecting duct cells. Am J Physiol Renal Physiol 2017; 313: F30-F46.
[69] Du L, Li J, Tian Y and Feng R. Pleckstrin-2-promoted PPM1B degradation plays an important role in transforming growth factor-β-induced breast cancer cell invasion and metastasis. Cancer Sci 2023; 114: 2429-2444.
[70] Ma Z, Lou S and Jiang Z. PHLDA2 regulates EMT and autophagy in colorectal cancer via the PI3K/AKT signaling pathway. Aging (Albany NY) 2020; 12: 7985-8000.
[71] Bonatto N, Carlini MJ, de Bessa Garcia SA and Nagai MA. PHLDA1 (pleckstrin homology-like domain, family A, member 1) knockdown promotes migration and invasion of MCF10A breast epithelial cells. Cell Adh Migr 2018; 12: 37-46.
[72] Xuan DTM, Wu CC, Kao TJ, Ta HDK, Anuraga G, Andriani V, Athoillah M, Chiao CC, Wu YF, Lee KH, Wang CY and Chuang JY. Prognostic and immune infiltration signatures of proteasome 26S subunit, non-ATPase (PSMD) family genes in breast cancer patients. Aging (Albany NY) 2021; 13: 24882-24913.
[73] Datta A, Deng S, Gopal V, Yap KC, Halim CE, Lye ML, Ong MS, Tan TZ, Sethi G, Hooi SC, Kumar AP and Yap CT. Cytoskeletal dynamics in epithelial-mesenchymal transition: insights into therapeutic targets for cancer metastasis. Cancers (Basel) 2021; 13: 1882.
[74] Leggett SE, Hruska AM, Guo M and Wong IY. The epithelial-mesenchymal transition and the cytoskeleton in bioengineered systems. Cell Commun Signal 2021; 19: 32.
[75] He Y, Zheng W, Huo Y, Sa L, Zhang H, He G and Shang P. PLEKHA4 promotes glioblastoma progression through apoptosis inhibition, tumor cell migration, and macrophage infiltration. Immunobiology 2023; 228: 152746.
[76] Zhi W, Wang Y, Jiang C, Gong Y, Chen Q, Mao X, Deng W and Zhao S. PLEKHA4 is a novel prognostic biomarker that reshapes the tumor microenvironment in lower-grade glioma. Front Immunol 2023; 14: 1128244.
[77] Palermo B, Franzese O, Frisullo G, D'Ambrosio L, Panetta M, Campo G, D'Andrea D, Sperduti I, De Nicola F, Goeman F, Gallina F, Visca P, Facciolo F and Nisticò P. CD28/PD1 co-expression: dual impact on CD8(+) T cells in peripheral blood and tumor tissue, and its significance in NSCLC patients' survival and ICB response. J Exp Clin Cancer Res 2023; 42: 287.
[78] Li T, Shi J, Wang L, Qin X, Zhou R, Dong M, Ren F, Li X, Zhang Z, Chen Y, Liu Y, Piao Y, Shi Y, Xu S, Chen J and Li J. Thymol targeting interleukin 4 induced 1 expression reshapes the immune microenvironment to sensitize the immunotherapy in lung adenocarcinoma. MedComm (2020) 2023; 4: e355.

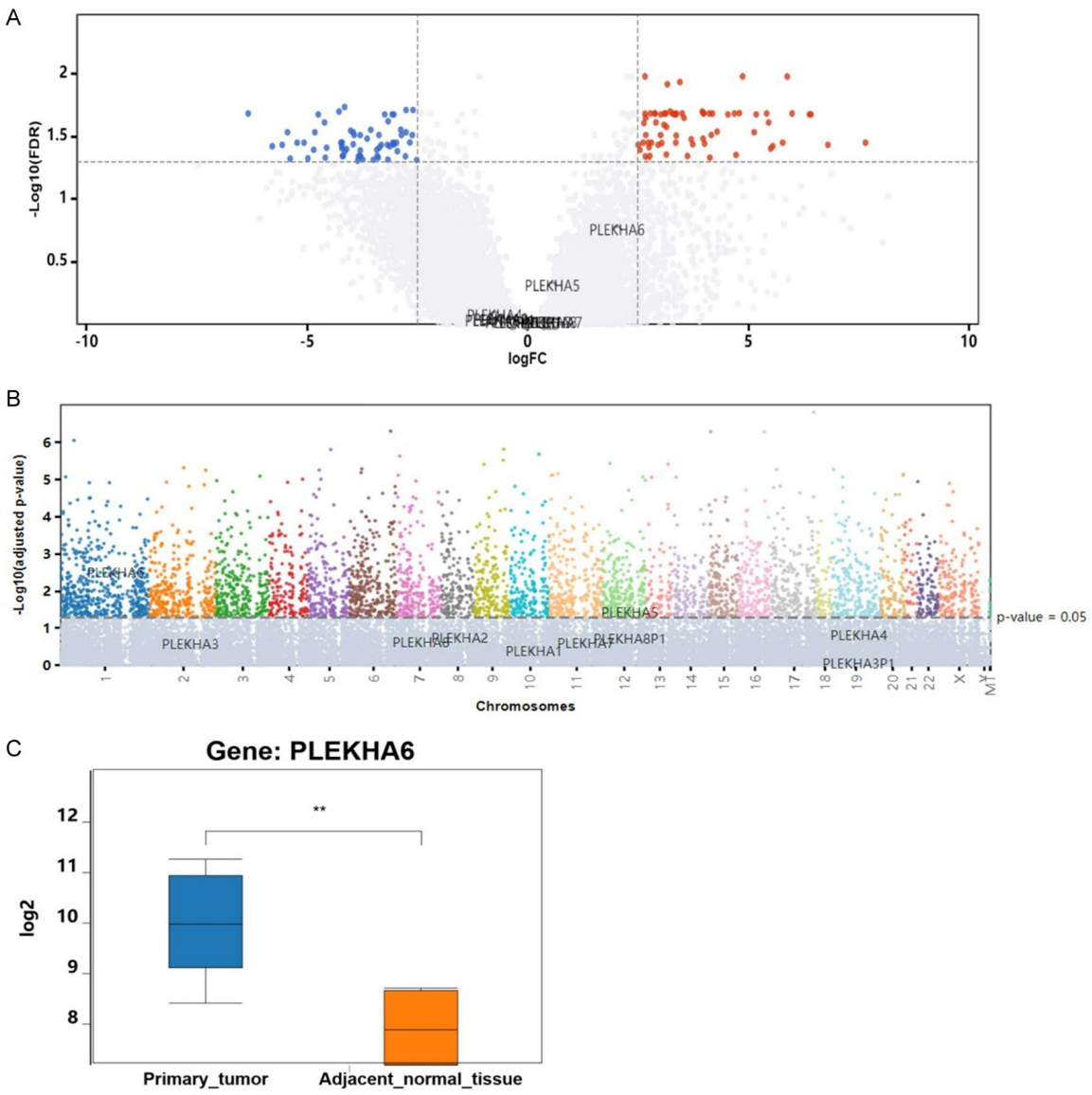

Supplementary Figure 1. Clinical transcriptomic validation of PLEKHA6 in LUAD. A. Volcano Plot highlighting PLEKHA gene family using Limma DEG analysis (cutoff value Log2 FC = ±2, *p*-value = 0.5). B. Manhattan plot of the samples with cutoff value being *p*-value < 0.05. C. Box-plot of PLEKHA6 expression comparison between tumor and normal sample using Tukey's t-test showing high significance between difference of expression (*p*-value < 0.0031451).

CELL LINE	PLEKHA6
HCC78	3.27
NCIH2106	3.05
CPCN	2.56
NCIH2029	2.43
NCIH446	2.42
NCIH2170	2.28
NCIH1944	2.28
NCIH1435	2.25
SQ1	2.20
NCIH1694	1.80
NCIH1385	1.72
NCIH854	1.69
NCIH2228	1.66
NCIH2347	1.65
NCIH2110	1.61
NCIH810	1.57
CALU3	1.56
COLO668	1.55
NCIH441	1.48
LU65	1.45
CORL95	1.44
DV90	1.43
BEN	1.40
SKLU1	1.38
DMS153	1.37
VMRCLCD	1.32
NCIH1651	1.30
NCIH2405	1.29
LCLC97TM1	1.29
NCIH2126	1.26
RERFLCAD1	1.25
NCIH1869	1.16
NCIH1618	1.12
HCC827	1.12
NCIH727	1.08
PC14	1.06
NCIH1838	1.06
DMS79	1.02
NCIH1105	0.99
DMS53	0.96
CALU1	0.94
CORL24	0.93
NCIH196	0.91
RERFLCAD2	0.90
SW900	0.87
CORL88	0.85
NCIH1573	0.80
NCIH2444	0.80
NCIH2122	0.80
NCIH1341	0.79
RERFLCKJ	0.72
NCIH1373	0.71
A549	0.68
VMRCLCP	0.63
DMS454	0.63

CELL LINE	PLEKHA6
HCC1171	0.61
KNS62	0.61
NCIH2291	0.60
NCIH2171	0.59
NCIH2023	0.57
NCIH1792	0.57
HCC4006	0.49
NCIH596	0.43
NCIH1734	0.42
NCIH526	0.42
NCIH209	0.41
NCIH146	0.40
NCIH1648	0.40
NCIH3255	0.40
EBC1	0.38
LCLC103H	0.36
NCIH2087	0.33
NCIH1092	0.33
NCIH2141	0.33
LOUNH91	0.32
HCC33	0.32
NCIH2342	0.32
NCIH1755	0.27
NCIH1437	0.27
ABC1	0.25
NCIH1436	0.23
HLFA	0.23
NCIH1836	0.20
NCIH510	0.18
LU99	0.18
NCIH2196	0.14
HCC44	0.12
CAL12T	0.12
CORL23	0.11
NCIH1184	0.08
HCC2935	0.06
NCIH2081	0.04
NCIH1568	0.03
NCIH1666	-0.01
NCIH647	-0.05
LXF289	-0.07
NCIH1930	-0.08
NCIH2066	-0.09
NCIH1563	-0.15
EPLC272H	-0.17
NCIH358	-0.17
SKMES1	-0.18
SCLC21H	-0.22
CALU6	-0.25
NCIH2009	-0.34
NCIH1975	-0.35
NCIH1963	-0.35
MORCPR	-0.35
NCIH2227	-0.39
NCIH1915	-0.40

CELL LINE	PLEKHA6
HCC2279	-0.44
NCIH524	-0.46
RERFLCMS	-0.46
NCIH2030	-0.47
NCIH1876	-0.47
NCIH1623	-0.52
HS618T	-0.57
NCIH226	-0.58
NCIH889	-0.60
HS229T	-0.60
HCC366	-0.60
HCC15	-0.61
NCIH211	-0.63
CHAGOK1	-0.64
NCIH1048	-0.65
NCIH1355	-0.65
NCIH1650	-0.67
LC1F	-0.70
LUDLU1	-0.72
NCIH522	-0.73
NCIH2172	-0.74
LC1SQSF	-0.74
NCIH1793	-0.75
SHP77	-0.76
DMS114	-0.78
RERFLCAI	-0.78
NCIH838	-0.79
NCIH1299	-0.80
SW1573	-0.80
NCIH1339	-0.80
HCC1195	-0.80
HARA	-0.81
NCIH520	-0.83
SBC5	-0.83
CORL47	-0.84
SW1271	-0.84
NCIH82	-0.85
NCIH2286	-0.86
DMS273	-0.86
CORL51	-0.88
NCIH1693	-0.90
NCIH1781	-0.91
NCIH23	-0.92
RERFLCSQ1	-0.94
NCIH841	-0.97
NCIH650	-0.99
NCIH460	-1.01
CORL279	-1.03
IALM	-1.03
NCIH661	-1.03
NCIH1581	-1.03
HCC95	-1.08
NCIH1703	-1.10
LK2	-1.12
NCIH69	-1.21

Supplementary Figure 2. PLEKHA6 mRNA expression landscape across LUAD cell lines. Heatmap showing PLEKHA6 mRNA expression levels across LUAD cell lines using data from the Cancer Cell Line Encyclopedia (CCLE). Expression values were obtained from the cBioPortal database and ranked accordingly. In the heatmap, red indicates higher expression and blue indicates lower expression.

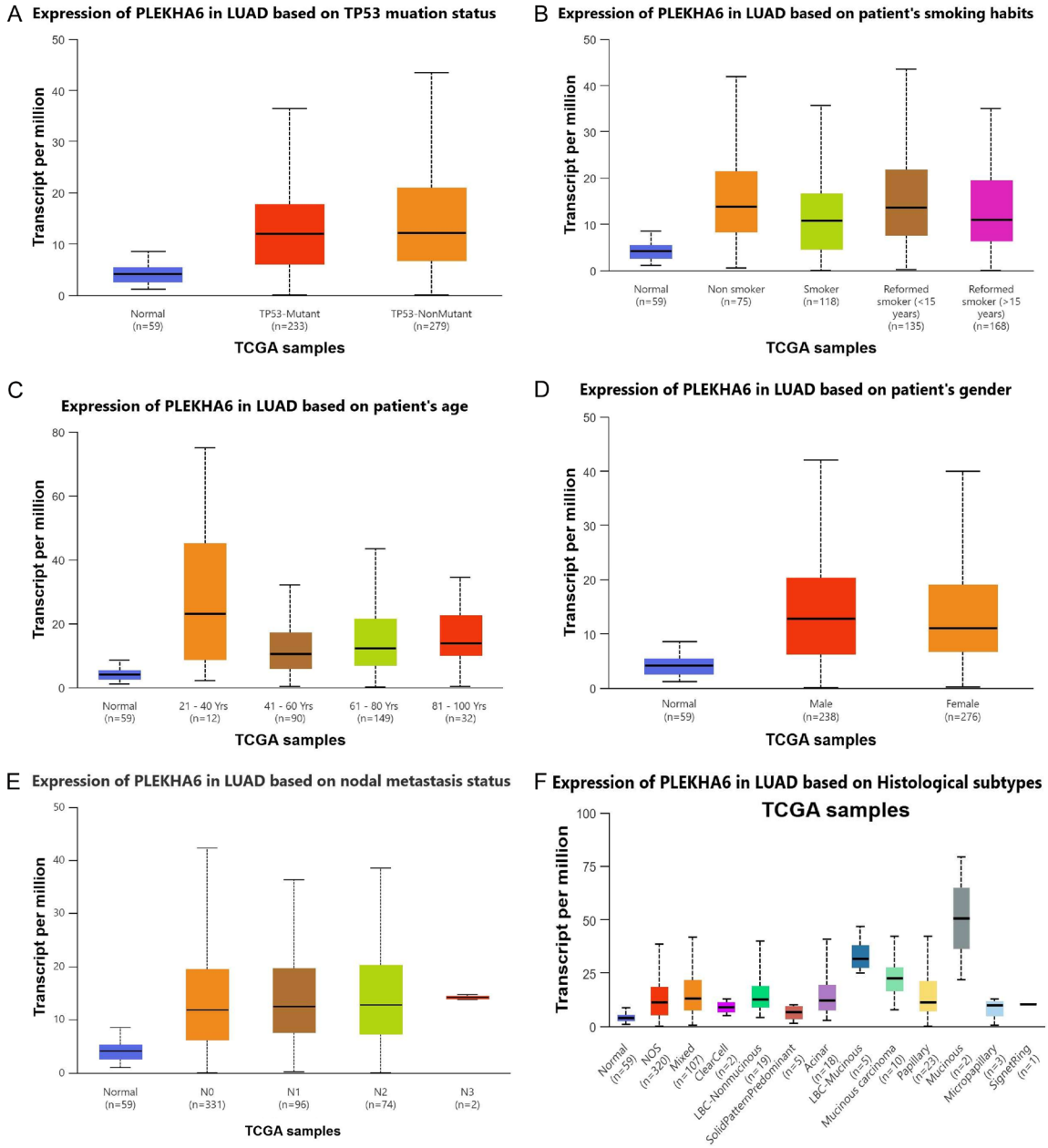

Supplementary Figure 3. Clinicopathological stratification of PLEKHA6 mRNA expression in LUAD. PLEKHA6 mRNA expression levels in LUAD patients stratified by various clinicopathological parameters: (A) TP53 mutation status; (B) smoking history; (C) patient age; (D) patient gender; (E) nodal metastasis status; and (F) Histological subtype.

Supplementary Table 1. Statistical expression of PLEKHA6 in LUAD based on sample types

Comparison	Statistical significance
Normal-vs-Primary	< 1E-12

Supplementary Table 2. Statistical expression of PLEKHA6 in LUAD based on TP53 mutation status

Comparison	Statistical significance
Normal-vs-TP53-Mutant	1.62436730732907E-12
Normal-vs-TP53-NonMutant	1.11022302462516E-16
TP53-Mutant-vs-TP53-NonMutant	7.723700E-02

Supplementary Table 3. Statistical expression of PLEKHA6 in LUAD based on patient's gender

Comparison	Statistical significance
Normal-vs-Male	1.62436730732907E-12
Normal-vs-Female	1.62447832963153E-12
Male-vs-Female	1.419410E-01

Supplementary Table 4. Statistical expression of PLEKHA6 in LUAD based on patient's smoking habits

Comparison	Statistical significance
Normal-vs-Non smoker	6.66355859380019E-13
Normal-vs-Smoker	3.65119046108475E-12
Normal-vs-Reformed smoker1	1.62447832963153E-12
Normal-vs-Reformed smoker2	1.62447832963153E-12
Nonsmoker-vs-Smoker	1.337590E-02
Nonsmoker-vs-Reformed smoker1	9.639600E-01
Nonsmoker-vs-Reformed smoker2	4.367700E-02
Smoker-vs-Reformed smoker1	5.000700E-03
Smoker-vs-Reformed smoker2	4.164000E-01
Reformed smoker1-vs-Reformed smoker2	1.486210E-02

Supplementary Table 5. Statistical expression of PLEKHA6 in LUAD based on Histological subtypes

Comparison	Statistical significance
Normal-vs-NOS	1.62436730732907E-12
Normal-vs-Mixed	< 1E-12
Normal-vs-ClearCell	4.503200E-01
Normal-vs-LBC-NonMucinous	4.413300E-04
Normal-vs-SolidPatternPredominant	2.038800E-01
Normal-vs-Acinar	1.537090E-03
Normal-vs-LBC-Mucinous	2.615800E-02
Normal-vs-Mucinous carcinoma	2.194100E-04
Normal-vs-Papillary	2.502600E-03
Normal-vs-Mucinous	3.522000E-01
Normal-vs-Micropapillary	4.631800E-01
Normal-vs-SignetRing	N/A
NOS-vs-Mixed	6.096400E-03
NOS-vs-ClearCell	5.472400E-01

NOS-vs-LBC-Non-Mucinous	7.803700E-02
NOS-vs-Solid Pattern Predominant	3.184400E-01
NOS-vs-Acinar	2.090800E-01
NOS-vs-LBC-Mucinous	2.796500E-03
NOS-vs-Mucinous carcinoma	2.680900E-03
NOS-vs-Papillary	3.962800E-01
NOS-vs-Mucinous	4.176200E-01
NOS-vs-Micropapillary	3.471200E-01
NOS-vs-Signet Ring	N/A
Mixed-vs-ClearCell	3.804400E-01
Mixed-vs-LBC-Non-Mucinous	8.882400E-01
Mixed-vs-Solid Pattern Predominant	1.568570E-01
Mixed-vs-Acinar	8.010800E-01
Mixed-vs-LBC-Mucinous	9.847700E-02
Mixed-vs-Mucinous carcinoma	1.610610E-01
Mixed-vs-Papillary	7.907800E-01
Mixed-vs-Mucinous	4.536200E-01
Mixed-vs-Micropapillary	2.194600E-01
Mixed-vs-Signet Ring	N/A
Clear Cell-vs-LBC-Non-Mucinous	3.802600E-01
Clear Cell-vs-Solid Pattern Predo minant	9.668400E-01
ClearCell-vs-Acinar	4.216200E-01
ClearCell-vs-LBC-Mucinous	1.638390E-01
ClearCell-vs-Mucinous carcinoma	8.343900E-02
ClearCell-vs-Papillary	5.440600E-01
ClearCell-vs-Mucinous	2.855600E-01
ClearCell-vs-Micropapillary	8.387600E-01
ClearCell-vs-SignetRing	N/A
LBC-NonMucinous-vs-SolidPatternPredominant	1.644160E-01
LBC-NonMucinous-vs-Acinar	9.319600E-01
LBC-NonMucinous-vs-LBC-Mucinous	1.733770E-01
LBC-NonMucinous-vs-Mucinous carcinoma	2.564800E-01
LBC-NonMucinous-vs-Papillary	7.833800E-01
LBC-NonMucinous-vs-Mucinous	4.598000E-01
LBC-NonMucinous-vs-Micropapillary	2.270200E-01
LBC-NonMucinous-vs-SignetRing	N/A
SolidPatternPredominant-vs-Acinar	2.007800E-01
SolidPatternPredominant-vs-LBC-Mucinous	3.223600E-02
SolidPatternPredominant-vs-Mucinous carcinoma	1.120450E-02
SolidPatternPredominant-vs-Papillary	3.278200E-01
SolidPatternPredominant-vs-Mucinous	3.826600E-01
SolidPatternPredominant-vs-Micropapillary	8.354800E-01
SolidPatternPredominant-vs-SignetRing	N/A
Acinar-vs-LBC-Mucinous	2.421000E-01
Acinar-vs-Mucinous carcinoma	3.453600E-01
Acinar-vs-Papillary	7.363400E-01
Acinar-vs-Mucinous	4.646200E-01
Acinar-vs-Micropapillary	2.698000E-01
Acinar-vs-SignetRing	N/A

LBC-Mucinous-vs-Mucinous carcinoma	5.367200E-01
LBC-Mucinous-vs-Papillary	1.872180E-01
LBC-Mucinous-vs-Mucinous	2.859600E-01
LBC-Mucinous-vs-Micropapillary	7.777700E-02
LBC-Mucinous-vs-SignetRing	N/A
Mucinous carcinoma-vs-Papillary	2.348200E-01
Mucinous carcinoma-vs-Mucinous	5.218200E-01
Mucinous carcinoma-vs-Micropapillary	2.911600E-02
Mucinous carcinoma-vs-SignetRing	N/A
Papillary-vs-Mucinous	2.246300E-02
Papillary-vs-Micropapillary	3.901000E-01
Papillary-vs-SignetRing	N/A
Mucinous-vs-Micropapillary	3.765400E-01
Mucinous-vs-SignetRing	N/A
Micropapillary-vs-SignetRing	N/A

Supplementary Table 6. Statistical expression of PLEKHA6 in LUAD based on nodal metastasis status

Comparison	Statistical significance
Normal-vs-N0	1.62436730732907E-12
Normal-vs-N1	1.11022302462516E-16
Normal-vs-N2	8.19559975440143E-11
Normal-vs-N3	2.41149999968826E-09
N0-vs-N1	8.846000E-01
N0-vs-N2	7.173600E-01
N0-vs-N3	9.300200E-01
N1-vs-N2	6.704800E-01
N1-vs-N3	9.327200E-01
N2-vs-N3	8.800600E-01

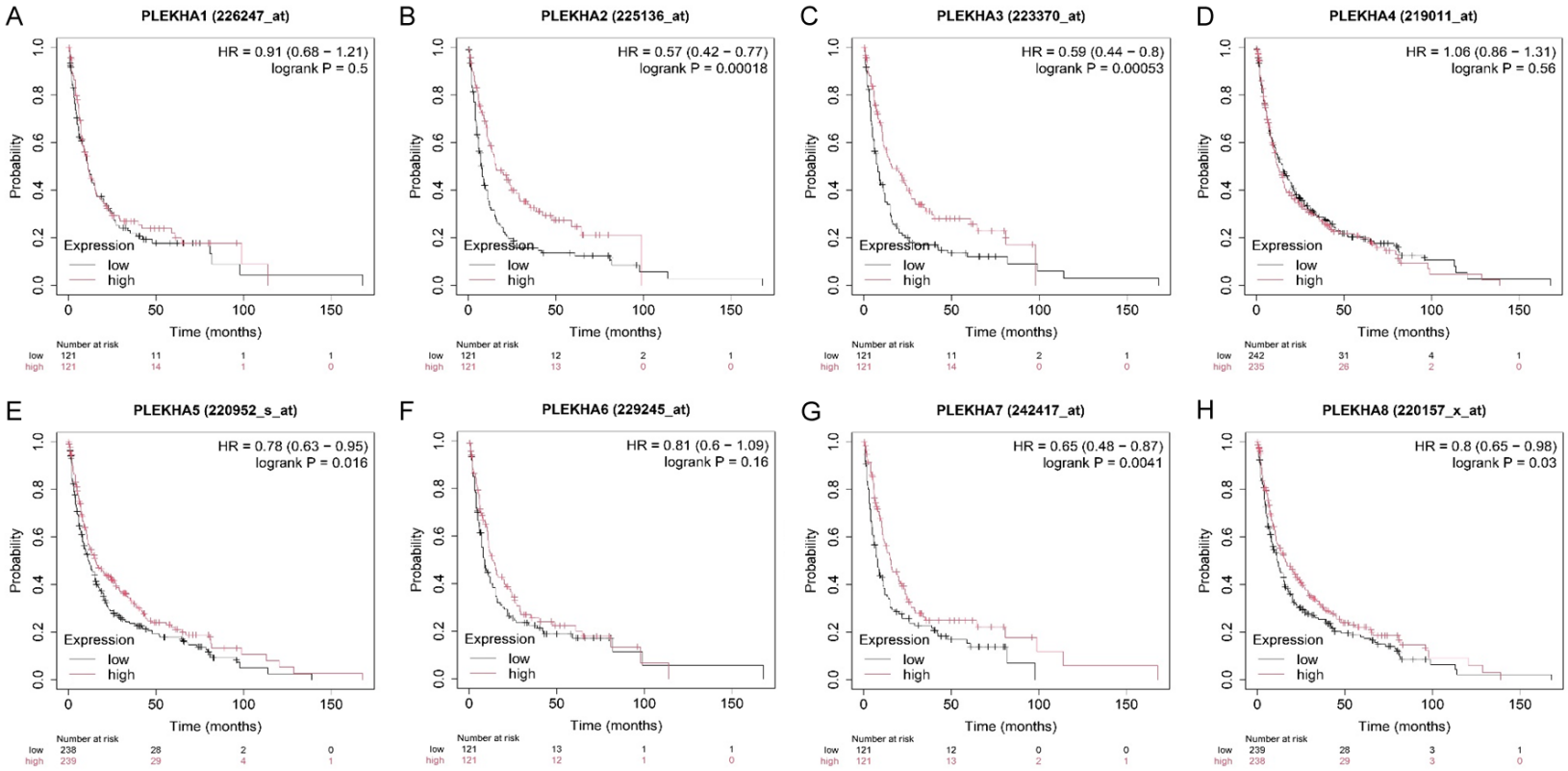

Supplementary Figure 4. Disease-free survival (DFS) analysis of PLEKHA gene family members in LUAD. Kaplan-Meier survival curves illustrating the association between mRNA expression levels of the eight PLEKHA genes and DFS in LUAD patients. Patients were stratified into high- and low-expression groups based on median expression levels.

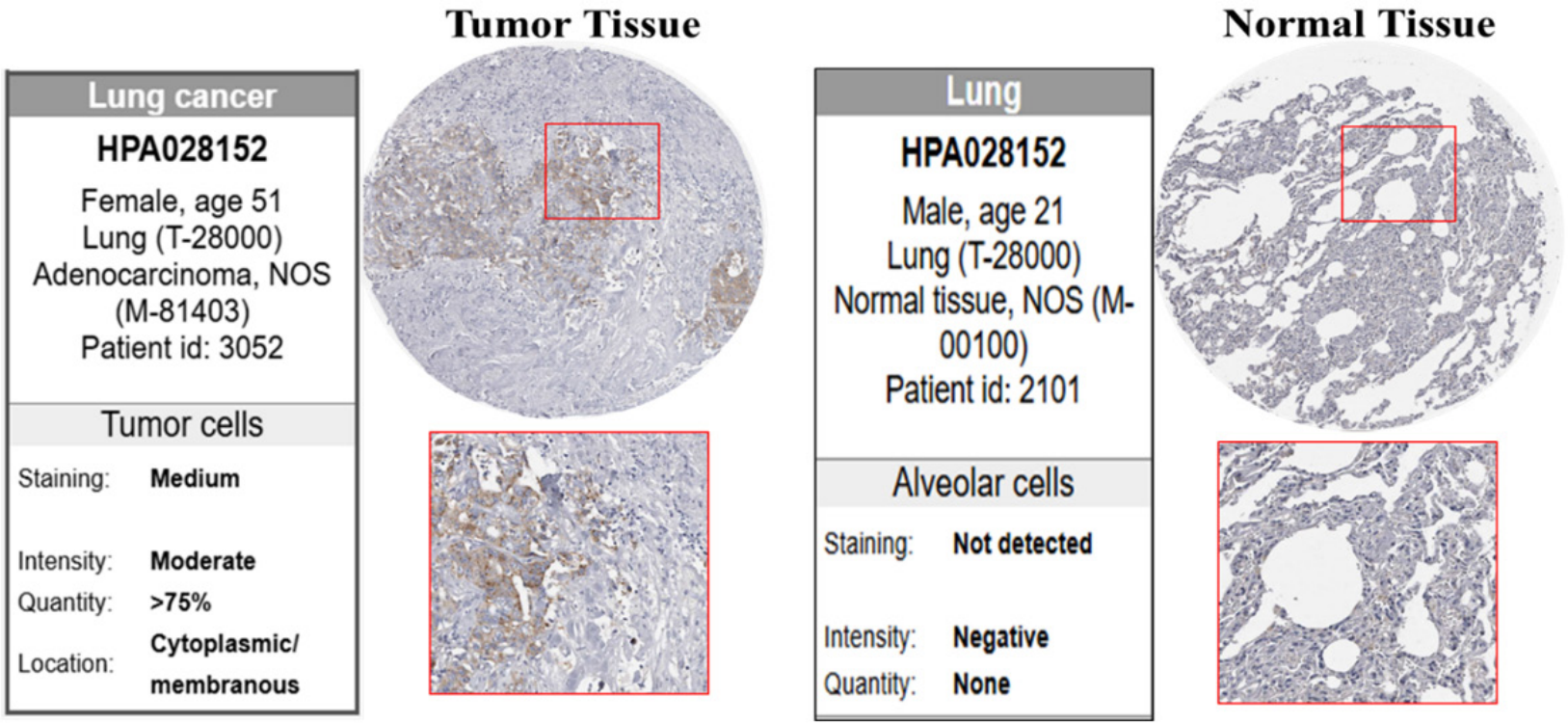

Supplementary Figure 5. Immunohistochemical validation of PLEKHA6 in LUAD. Immunohistochemical staining showing the expression of PLEKHA6 in normal lung tissues and Tumor Tissue.

Supplementary Table 7. Pathway analysis of genes co-expressed PLEKHA6 from TCGA LUAD databases using the MetaCore database (with *p*-value < 0.05 set as the cutoff value)

#	Maps	*p* Value	Network Objects from Active Data
1	Cell adhesion_Endothelial cell contacts by junctional mechanisms	1.56E-08	MAGI-1 (BAIAP1), Plakophilin 4, Alpha-actinin, Cingulin, Plakoglobin, p120-catenin, AF-6, ZO-1, Alpha-catenin, ZO-2
2	Signal transduction_Ephrin-B signaling	1.38E-07	Ephrin-B1, p130CAS, p190-RhoGEF, HGK (MAP4K4), PAK, PAK1, Kalirin, PICK1, AF-6, c-Src, Ephrin-B, GRB7
3	Cell adhesion_Classical cadherin-mediated cell adhesion	2.42E-07	MAGI-1 (BAIAP1), E-cadherin, Cortactin, Formin, Alpha-actinin, Plakoglobin, p120-catenin, Alpha-catenin, VAV-2
4	Cell adhesion_Tight junctions	4.62E-07	Cortactin, ZO-3, Cingulin, PDZ-RhoGEF, EPB41, Tubulin alpha, Claudin-2, AF-6, ZO-1, DNMBP (TUBA), ZO-2
5	PXR-mediated direct regulation of xenobiotic metabolizing enzymes/Rodent version	1.20E-06	UGT1A3, CYP2C19, MRP3, UGT1A1, CYP3A4, SR-BI, CES2, UGT1A4, CYP3A5, UGT1A6
6	Cytoskeleton remodeling_Regulation of actin cytoskeleton organization by the kinase effectors of Rho GTPases	1.26E-06	BETA-PIX, Cortactin, Alpha-actinin, MRCKalpha, PAK, PAK1, MyHC, LIMK, Spectrin, SLC9A1, MRCK, PRK1
7	Androstenedione and testosterone biosynthesis and metabolism p.2	1.77E-06	UGT1A3, UGT1A9, AKR1C3, UGT1A1, AKR1C4, UGT1A10, UGT1A8, UGT1A4, UGT2B15
8	PXR-mediated direct regulation of xenobiotic metabolizing enzymes/Human version	2.51E-06	UGT1A3, CYP2C19, MRP3, UGT1A1, CYP3A4, SR-BI, CES2, UGT1A4, CYP3A5, UGT1A6
9	G-protein signaling_RhoA activation	3.45E-06	IGF-1 receptor, p190-RhoGEF, DBS, Cingulin, PDZ-RhoGEF, Ephexin, Thrombin, Ephrin-A, Plexin B2, Angiotensin II, ACM1, c-Src, ZO-1, VAV-2
10	Neurophysiological process_Receptor-mediated axon growth repulsion	6.08E-06	Cortactin, PDZ-RhoGEF, Ephexin, LIMK2, PAK1, Ephrin-A, Plexin A2, c-Src, GRB7, VAV-2
11	Protein folding and maturation_Angiotensin system maturation	9.12E-06	Angiotensin III, Angiotensin (2-10), Angiotensinogen, Angiotensin IV, Angiotensin I, Angiotensin II, Kallikrein 1, Angiotensin (1-7), Angiotensin (1-9), ACE2
12	Inhibition of Ephrin receptors in colorectal cancer	1.04E-05	Ephrin-B1, E-cadherin, SMAD3, Ephrin-A, KLF5, Ephrin-B, Frizzled, VAV-2
13	G-protein signaling_Rac1 activation	1.79E-05	BETA-PIX, p130CAS, DOCK6, PAK, EPS8, ErbB2, p200RhoGAP, Kalirin, AF-6, c-Src, FARP2, VAV-2
14	Effect of H. pylori infection on gastric epithelial cells motility	2.02E-05	E-cadherin, Cortactin, Alpha-actinin, PAK1, p120-catenin, c-Src, Connexin 32, ZO-1, Alpha-catenin
15	Estradiol metabolism	2.02E-05	UGT1A3, CYP2C19, UGT1A1, CYP3A4, UGT1A10, UGT2B7, SULT1A3, UGT1A4, CYP3A5
16	E-cadherin signaling and its regulation in gastric cancer	4.43E-05	E-cadherin, Formin, Alpha-actinin, Plakoglobin, p120-catenin, c-Src, Alpha-catenin, Frizzled
17	Retinol metabolism	5.40E-05	DGAT1, UGT1A3, CYP2C19, CYP2C18, CYP3A4, UGT2B7, BCDO, Xanthine oxidase, UGT1A8, CYP3A5, RDH5
18	Signal transduction_Ephrin reverse signaling	5.97E-05	Ephrin-B1, PAK1, Ephrin-A, PICK1, SFK, c-Src, Ephrin-B
19	2-Naphthylamine and 2-Nitronaphtalene metabolism	7.02E-05	UGT1A3, UGT1A9, UGT1A1, GSTA5, CYP3A4, GSTA1, SULT1A3, UGT1A8, UGT1A4, UGT1A6
20	Retinoic acid maintains mucocilliary differentiation and mucins expression in normal and asthmatic airway epithelium	9.61E-05	Mucin 5B, Mucin 4, MUC1, Thyroid hormone receptor, SP1, Mucin 2, GCNT3
21	CAR-mediated direct regulation of xenobiotic metabolizing enzymes/Rodent version	9.87E-05	CYP2C19, MRP3, UGT1A1, CYP3A4, NQO1, ADHG, CYP3A5, UGT1A6
22	CAR-mediated direct regulation of xenobiotic metabolizing enzymes/Human version	9.87E-05	CYP2C19, MRP3, UGT1A1, CYP3A4, NQO1, ADHG, CYP3A5, UGT1A6

23	Cell adhesion_Gap junctions	1.21E-04	Connexin 36, E-cadherin, Tubulin alpha, Connexin 32, ZO-1, ZO-2
24	G-protein signaling_CDC42 activation	1.41E-04	BETA-PIX, E-cadherin, DOCK6, DBS, BCR, c-Src, FARP2, DNMBP (TUBA), Frabin, VAV-2
25	G-protein signaling_CDC42 inhibition	2.04E-04	RhoGAP1, ABR, BCR, p200RhoGAP, RalBP1, GRAF
26	Cell adhesion_Histamine H1 receptor signaling in the interruption of cell barrier integrity	2.35E-04	p130CAS, E-cadherin, Alpha-actinin, LIMK2, p120-catenin, c-Src, ZO-1, Alpha-catenin
27	G-protein signaling_RhoB activation	2.83E-04	p190-RhoGEF, DBS, PDZ-RhoGEF, SMAD3, TRIF (TICAM1), TIM1, p300, FOXO3A, VAV-2
28	Inhibition of TGF-beta signaling in gastric cancer	3.28E-04	CEACAM5, SMAD3, Sin3A, p300, Beta-fodrin, ELF3
29	Regulation of metabolism_ChREBP signaling	4.72E-04	RETSAT, ACACA, Sin3A, TUG1, p300, HNF4-alpha, PCSK9, ROR-gamma, PPAR-alpha
30	Acetaminophen metabolism	5.33E-04	UGT1A3, UGT1A9, MRP3, UGT1A1, CYP3A4, UGT1A10, NQO1, UGT2B15, UGT1A6
31	O-glycan biosynthesis	5.33E-04	GALNT4, B3GT2, GALNTL2, GALNT12, SIA7A, GALNT2, GCNT3, GALNT7, B3GT5
32	Bone metastases in Prostate Cancer	6.15E-04	LRP5, IGF-1 receptor, ErbB2, c-Src, Frizzled, Kallikrein 3 (PSA)
33	Immune response_BAFF-induced non-canonical NF-kB signaling	7.44E-04	Skp2/TrCP/FBXW, UBE1, TRAF3, UEV1A, Furin, beta-TrCP
34	Oxidative stress_Activation of NOX1, NOX5, DUOX1 and DUOX2 NADPH Oxidases	8.63E-04	DUOXA2, BETA-PIX, DUOX2, DUOX1, c-Src, DUOXA1, VAV-2
35	Development_WNT/Beta-catenin signaling in the cytoplasm	9.55E-04	E-cadherin, Axin1, PAK1, p120-catenin, c-Src, Axin, Frizzled, VAV-2
36	1-Naphthylamine and 1-Nitronaphtalene metabolism	1.32E-03	UGT1A3, UGT1A9, UGT1A1, GSTA1, UGT1A8, UGT1A4, UGT1A6
37	Role of alpha-6/beta-4 integrins in cancer progression	1.32E-03	Plectin 1, ITGB4, MSP receptor (RON), ErbB2, PAK1, IRS-2, ErbB3
38	Cell adhesion_Endothelial cell contacts by non-junctional mechanisms	1.71E-03	MAGI-1(BAIAP1), Alpha-actinin, Plakoglobin, p120-catenin, Alpha-catenin
39	Regulation of lipid metabolism_Cholesterol regulation of lipidic metabolism	1.73E-03	ACACA, NPC1L1, SREBP2 (nuclear), CYP3A4, p300, SR-BI, SREBP2 precursor, PCSK9, SREBP2 (Golgi membrane)
40	Pro-oncogenic action of Androgen receptor in breast cancer	1.74E-03	E-cadherin, AKR1C3, MUC1, ErbB2, Kallikrein 3 (PSA), ErbB3
41	Development_Trophectoderm differentiation	2.07E-03	SMAD3, Furin, PACE4, CDX2, CRIPTO
42	Development_Positive regulation of WNT/Beta-catenin signaling in the cytoplasm	2.09E-03	IGF-1 receptor, Bcl-9, SMAD3, IRS-2, Insulin receptor, Axin, USP7, Alpha-1 catenin, Frizzled
43	Apoptosis and survival_NGF/ TrkA PI3K-mediated signaling	2.29E-03	BETA-PIX, MRCKalpha, LIMK2, PAK1, Kalirin, c-Src, ARAP3, FOXO3A, VAV-2
44	Cell adhesion_Cell-matrix glycoconjugates	2.69E-03	CEACAM5, Galectin-4, BCAN, MUC1, ITIH2, A1M
45	Regulation of metabolism_Glucocorticoid receptor signaling in glucose and lipid metabolism	2.98E-03	FACVL1, HNF3-gamma, ACACA, G6PE, Sin3A, p300, SREBP2 precursor, HNF3, FOXO3A
46	G-protein signaling_Rac3 regulation pathway	3.15E-03	ABLIM1, Neurabin-1, PAK1, HNF1-alpha
47	Development_Negative regulation of WNT/Beta-catenin signaling in the cytoplasm	3.24E-03	E-cadherin, Skp2/TrCP/FBXW, CXXC5, CXXC4, Axin, beta-TrCP, Alpha-1 catenin, Frizzled, Beclin 1
48	Development_ErbB4 signaling	3.46E-03	Neuregulin 4, N-CoR, ErbB2, Kalirin, SFK, c-Src, S100B, GRB7
49	Androstenedione and testosterone biosynthesis and metabolism p.3	3.51E-03	UGT1A9, AKR1C3, AKR1C4, UGT1A10, UGT2B7, UGT2B4
50	NRF2 regulation of oxidative stress response	3.85E-03	MafK, GPX2, UGT1A1, GSTA1, MafF, NQO1, SLC7A11

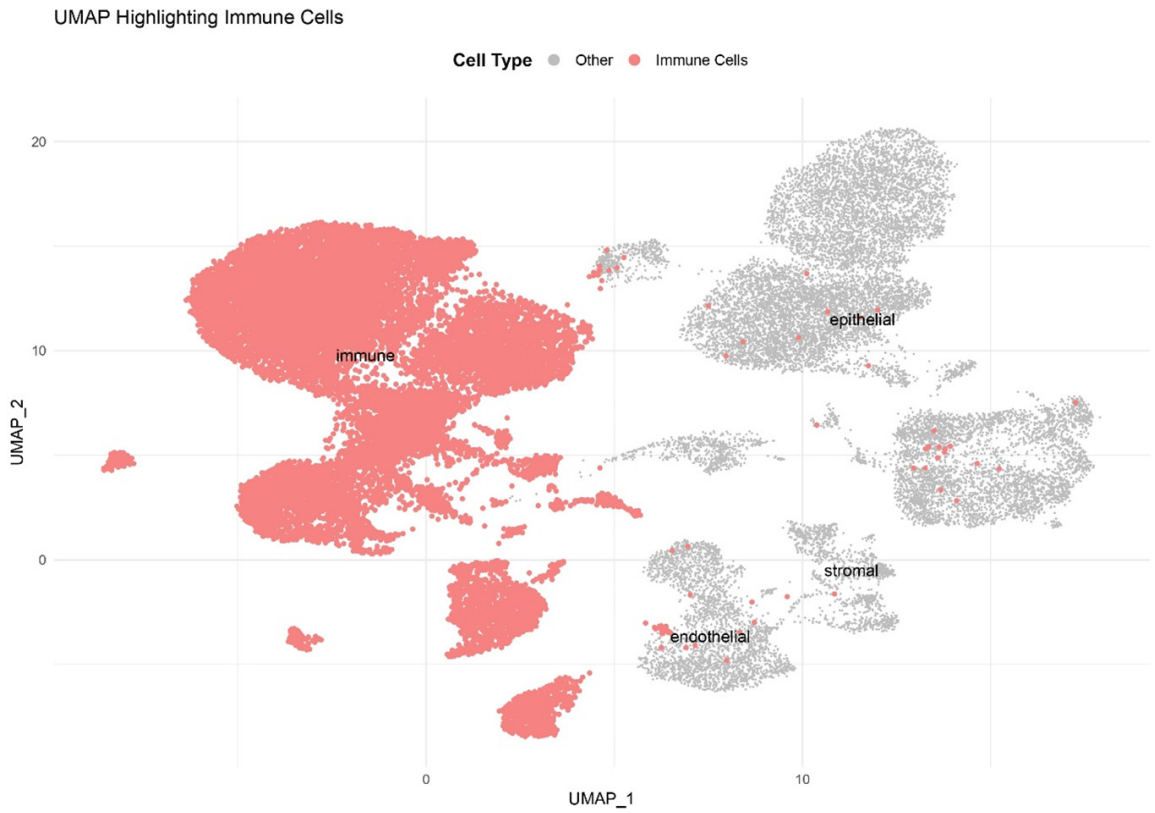

Supplementary Figure 6. Single-cell transcriptomic mapping of PLEKHA6 in LUAD microenvironment. This UMAP plot visualizes the distribution of cell types in LUAD tissue based on single-cell transcriptomic data, with a focus on PLEKHA6 expression. Immune cells, highlighted in red, form a distinct cluster on the left side of the plot, while other cell types, including epithelial (top right), stromal (bottom right), and endothelial cells (center-bottom), are shown in gray. The clustering pattern suggests a spatial and transcriptional distinction of immune cells, potentially implicating PLEKHA6 in immune-related functions within the LUAD tumor microenvironment.